PAPER

Synthesis, characterization and biological evaluation of formononetin derivatives as novel EGFR inhibitors *via* inhibiting growth, migration and inducing apoptosis in breast cancer cell line†

Hong-Yan Lin,‡[ab] Wen-Xue Sun,‡[ab] Chao-Sai Zheng,[ab] Hong-Wei Han,[ab] Xue Wang,[ab] Ya-Han Zhang,[ab] Han-Yue Qiu,[ab] Cheng-Yi Tang,[ab] Jin-Liang Qi,[ab] Gui-Hua Lu,[ab] Rong-Wu Yang,*[ab] Xiao-Ming Wang [ID] *[ab] and Yong-Hua Yang [ID] *[ab]

Over the past few decades, the human epidermal growth factor receptor (EGFR) has been established as an attractive target for non-small cell lung cancer (NSCLC) therapy. Nevertheless, the approved EGFR inhibitors, gefitinib or erlotinib have shown minimum clinical activity to breast cancer patients, who also highly expressed EGFR. In this study, we designed and synthesized a series of novel formononetin derivatives by reference to the binding mode of lapatinib to EGFR. *In vitro* EGFR and cell growth inhibition assay demonstrated that compound **4v** exhibited the most potent anti-EGFR (IC_{50} = 14.5 nM) and anti-proliferation activity (IC_{50} = 5.44 ± 1.28 μM) against MDA-MB-231 cell line, which was comparable to that of lapatinib (EGFR, IC_{50} = 5.6 nM; MDA-MB-231, IC_{50} = 2.48 ± 1.04 μM). Further biological experiment results demonstrated that **4v** could effectively induce apoptosis, inhibit proliferation and migration in MDA-MB-231 cells through targeting EGFR and then blocking the downstream signaling pathways, EGFR/PI3K/Akt/Bad, EGFR/ERK and EGFR/PI3K/Akt/β-catenin, respectively. However, it had no significant influence on cell cycle distribution and the related proteins (Cyclin A, Cyclin D1, CDK4) expression. *In vivo* anti-tumor results also preliminarily confirmed the effectiveness of **4v** in tumor chemotherapy in mice and indicated its potential as a new EGFR inhibitor in the treatment of MDA-MB-231 malignant tumor.

Introduction

The epidermal growth factor receptor (EGFR) is a transmembrane protein, belonging to the family of tyrosine kinases and involved in cell proliferation and signal transduction.[1] It has been confirmed that EGFR is highly or abnormally expressed in many solid tumors and is correlated to tumor cell proliferation, angiogenesis, tumor invasion, metastasis, and inhibition of apoptosis.[2,3] Over-expression of EGFR is also crucial for the evolution of malignant tumors, such as glioma cell, kidney, lung, breast, prostate and pancreatic cancer.[4–6] The activation of EGFR phosphorylates its downstream signalling molecules PI3K and Akt, which are involved in cellular migration, apoptosis and mitogen-activated protein kinase signalling, Ras/Raf/MEK/ERK, as implicated in cell proliferation.[7,8] It is well known that inhibition of EGFR kinase-mediated signal is a well-established strategy for the treatment of advanced stage non-small cell lung cancer (NSCLC) and also correlated well with the proliferation and migration of aggressive triple negative breast cancer, MDA-MB-231.[9,10]

Studies have shown that triple-negative breast cancer was considered another potential indication for EGFR kinase inhibitors because they are not amenable to endocrine or HER-2 targeted therapies, while they highly-express EGFR kinase.[10,11] Some literatures have suggested a crucial role of EGFR in breast cancer proliferation and migration. However, inhibition of EGFR by gefitinib or erlotinib showed low efficacy in arresting tumor cell growth at the cell line level and minimum clinical activity.[7,12] Such extraordinary phenomenon always attracts us to explore the underlying mechanism and discover new potent EGFR inhibitors that are naturally derived chemicals as breast cancer therapeutics.

Natural products are a major source of drug discovery and cancer therapy. Formononetin (Fig. 1) is a bioactive isoflavone found in diverse Chinese medicine herbals, such as *Amorpha*

[a]*State Key Laboratory of Pharmaceutical Biotechnology, NJU-NJFU Joint Institute of Plant Molecular Biology, Nanjing University, Nanjing, 210023, China. E-mail: Yangyh@nju.edu.cn; Wangxm07@nju.edu.cn; Robertyang@nju.edu.cn; Fax: +86-25-89681381; Tel: +86-25-89681381*

[b]*Co-Innovation Center for Sustainable Forestry in Southern China, Nanjing Forestry University, Nanjing, 210037, China*

† Electronic supplementary information (ESI) available. See DOI: 10.1039/c7ra09825a

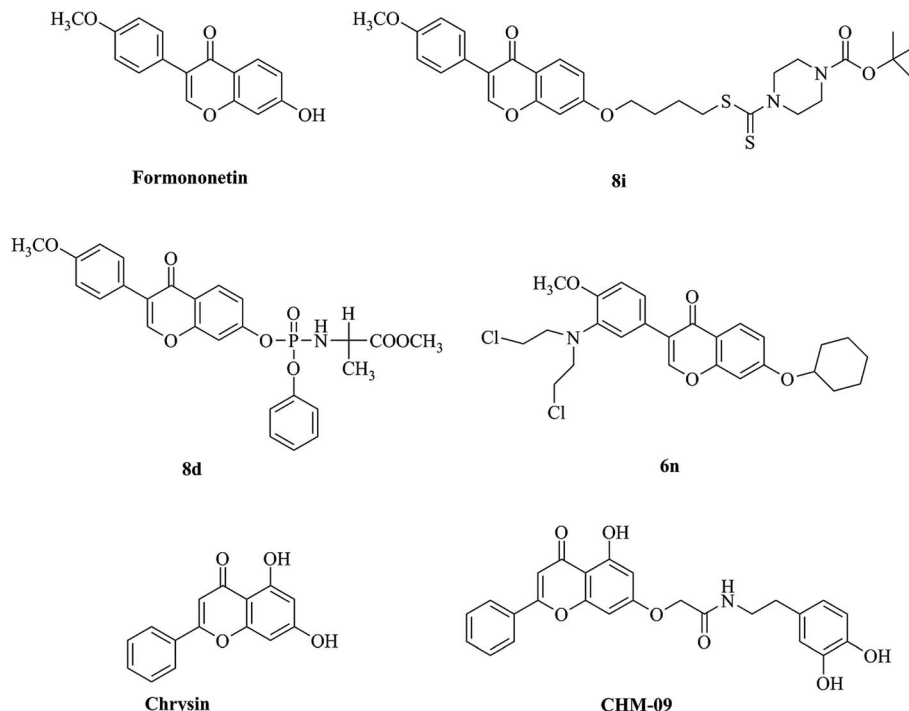‡ These two authors contribute equally to this article.

Fig. 1 Formononetin derivatives with anticancer activity.

fruticose,[13] *Glycyrrhiza*,[13,14] *Trifolium pretense*,[13,14] *Astragalus membranaceus*,[15] which belonging to the family of Leguminosae. It has attracted broad attention because of multiple pharmacological activities, such as anti-bacterial,[16,17] anti-cancer,[17] anti-oxidant,[18] anti-diabetic[19,20] and anti-hyperlipidemia.[21] Currently, many formononetin analogues (Fig. 1) were designed as anti-cancer agents and explored the biological mechanism against various human cancer cell lines. As reported that formononetin can induce cell apoptosis *via* PI3K/AKT signaling pathway in human nasopharyngeal and cervical carcinoma cells.[22] Formononetin–dithiocarbamate hybrids **8i** could inhibit growth and migration of PC-3 cells *via* MAPK/Wnt signaling pathway and cause cell cycle arrest in G1 phase.[23] While its 7-phosphoramidate derivative **8d** and nitrogen-mustard derivative **6n** could induce cell cycle arrest in G2/M phase and cell apoptosis.[24,25] In addition, Manupati *et al.* reported a chrysin analog CHM-09 which potentiated the mesenchymal–epithelial transition of breast cancer stem cells through inhibiting EGFR.[10] In the light of previous studies, we reported here the designation of novel formononetin derivatives as potent anticancer agents through targeting EGFR and further investigation of their underlying biological mechanisms.

Results and discussion

Chemistry

In this study, we hypothesize that the design of synthetic derivatives of formononetin against EGFR with lapatinib as positive control may improve its anticancer efficacy. Before synthesis, a molecular screening process was performed by computer assist drug design (CADD) method. Molecular docking was conducted to calculate the binding energy (CDOCKER INTERACTION ENERGY in CDOCKER protocol in Discovery Studio 3.5) between compounds and EGFR complex structure (1XKK.pdb, downloaded from the PDB). Finally, 22 compounds were picked to continue assays subsequently and their binding energy were shown in Table S1 (ESI†).

In view of the binding energy, **4v** is the best one among them. For better understanding of the potential of **4v**, we further examined the interaction of **4v** with EGFR (PDB code 1XKK) with lapatinib as the positive control. All the amino acid residues which had interactions with lapatinib were exhibited and the results were depicted in Fig. 2A. In the binding model, lapatinib bound well to EGFR mainly *via* three hydrogen bonds with ARG 803, ASP 800 and PHE856, a π-cation bond with LYS 745 and a π–π bond with PHE856. In the binding model of **4v** with EGFR (Fig. 2C), there formed a hydrogen bond with MET 793, a π-cation bond with LYS 745, a π-anion bond with ASP 800, a π–π bond with PHE856 and a π-sigma bond with MET766 which are the main contributors for the effective combination between them. The 3D models of the interaction between lapatinib, **4v** and EGFR were also depicted in Fig. 2B and D. For Fig. 2E, we further compared the structure and target combine similarity of **4v** and lapatinib. The result demonstrated that **1c** might be a potential EGFR inhibitor.

The synthetic routes of novel formononetin derivatives are outlined in Scheme 1, and structure of derivatives **4a–4v** are shown in Table 1. These compounds were obtained by three steps which were elucidated in the Experimental section. All of them are first reported and characterized by ^{1}H NMR, ^{13}C NMR, elemental analysis, melting test and mass spectroscopy, and results are in full accordance with their depicted structures.
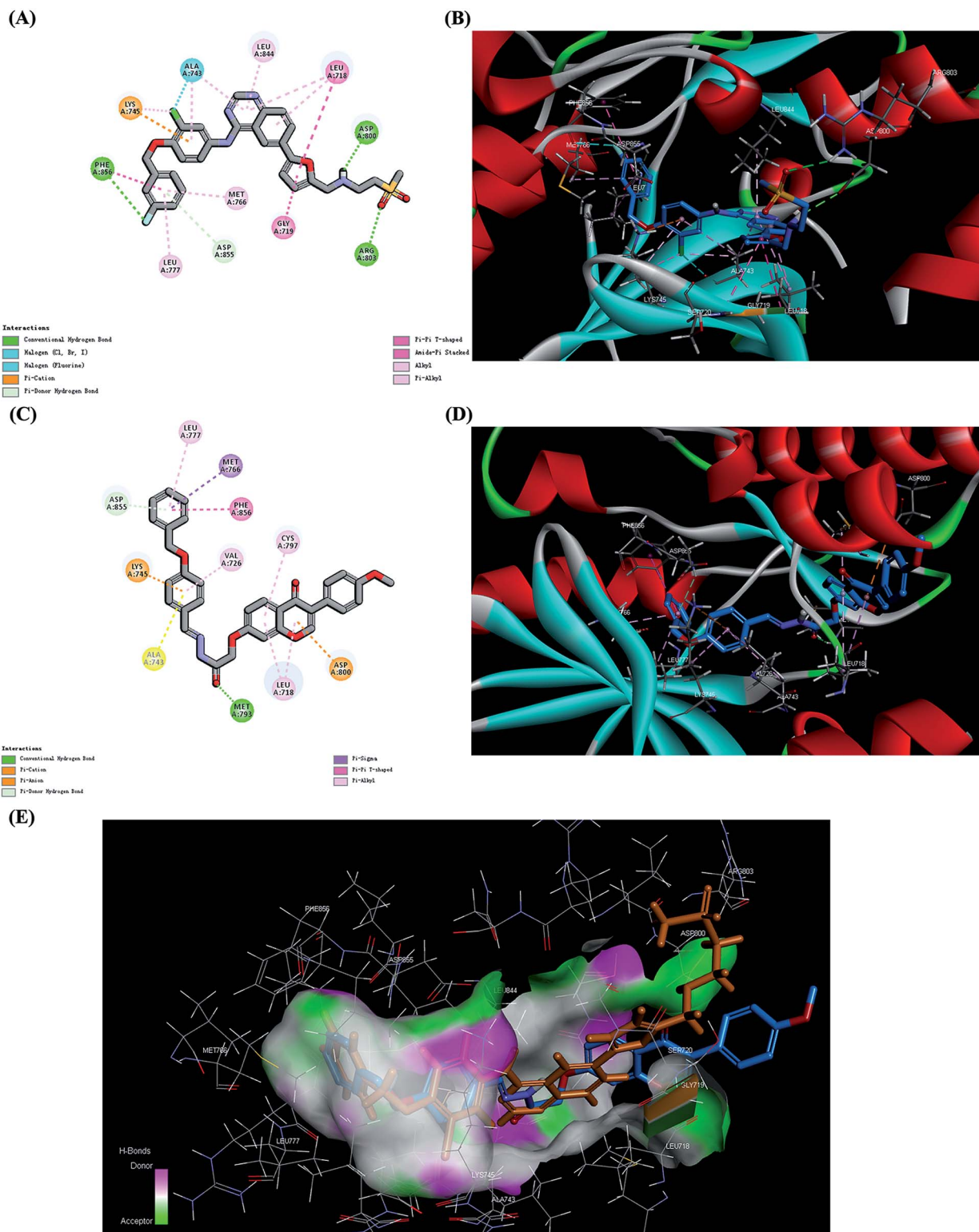
Fig. 2 Molecular docking analysis of **4v** and lapatinib, showing proposed binding modes with EGFR (PDB code 1XKK). (A) Interactions of lapatinib with the amino acid residues at the binding pocket of EGFR (carbon atom, gray; oxygen atom, red; hydrogen atom, white; nitrogen atom, purple; chlorine atom, bright green; fluorine atom, light green; sulphur atom, orange). (B) Binding pose of lapatinib in the protein surface of EGFR (carbon atom, blue; oxygen atom, red; hydrogen atom, white; nitrogen atom, purple; chlorine atom, bright green; fluorine atom, sulphur atom, orange). Hydrogen bonds were displayed as green dashed lines. (C) Interactions of **4v** with the amino acid residues at the binding pocket of EGFR (carbon atom, gray; oxygen atom, red; hydrogen atom, white; nitrogen atom, purple; sulphur atom, orange). (D) Binding pose of **4v** in the protein surface of EGFR (carbon atom, blue; oxygen atom, red; hydrogen atom, white; nitrogen atom, purple; sulphur atom, orange). Hydrogen bond was displayed as green dashed lines. (E) 3D mode of the interaction between the compounds (lapatinib, brown; **4v**, blue) and the EGFR binding site. The protein is represented by molecular surface.
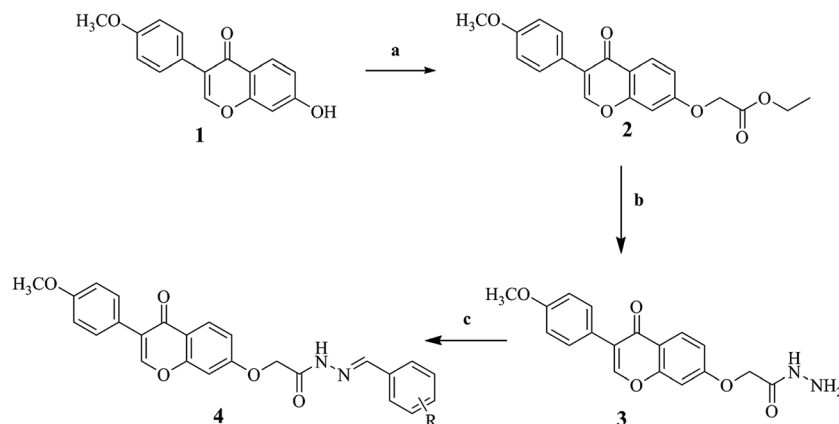
Scheme 1 Chemical synthesis routine of **4a–4v**. Reagents and conditions: (a) ethyl bromoacetate, acetone, K_2CO_3, reflux, 10 hours; (b) hydrazine hydrate, ethanol, reflux, 10 hours; (c) benzaldehyde, glacial acetic acid, ethanol, reflux, 6 hours.

Table 1 Chemical structures of **4a–4v**

Compound	R_1	R_2	R_3	R_4	R_5
4a	H	H	H	H	H
4b	F	H	H	H	H
4c	H	F	H	H	H
4d	H	H	F	H	H
4e	H	F	F	H	H
4f	Cl	H	H	H	H
4g	H	Cl	H	H	H
4h	H	H	Cl	H	H
4i	Cl	Cl	H	H	H
4j	Cl	H	H	H	Cl
4k	H	Br	H	H	H
4l	H	OH	H	H	H
4m	H	H	OH	H	H
4n	H	H	NH_2	H	H
4o	CF_3	H	H	H	H
4p	H	H	CF_3	H	H
4q	H	H	CH_3	H	H
4r	OCH_3	H	H	H	H
4s	H	H	OCH_3	H	H
4t	H	OCH_3	OCH_3	H	H
4u	H	H	$CH(CH_3)_2$	H	H
4v	H	H	OC_7H_7	H	H

compounds presented stronger EGFR inhibitory activity compared to formononetin itself. Especially, compound **4v** was the most potent inhibitor of EGFR ($IC_{50} = 14.5$ nM), which was at least 10-fold stronger than formononetin ($IC_{50} > 150$ nM) and almost comparable to gefitinib ($IC_{50} = 6.2$ nM) and lapatinib ($IC_{50} = 5.6$ nM). Among them, compound **4n** also showed potent EGFR inhibitory activity with an IC_{50} value of 20.6 nM. Generally, electron-donating group improved the enzymatic inhibitory activity more significantly than the electron-withdrawing group, especially when the substitution appeared at the R3-position of benzene ring of formononetin skeleton.

Table 2 The EGFR inhibitory activity of **4a–4v**, formononetin, gefitinib and lapatinib

Compound	EGFR kinase	
	% inhibition at 150 nM	IC_{50} (nM)
4a	54.7	120.4
4b	51.6	131.6
4c	33.5	>150
4d	70.3	52.6
4e	68.4	66.2
4f	52.3	142.2
4g	50.2	146.3
4h	72.8	30.7
4i	60.1	98.4
4j	58.5	105.8
4k	56.2	112.5
4l	50.9	139.5
4m	73.5	33.1
4n	75.7	20.6
4o	43.1	>150
4p	66.8	48.9
4q	70.4	30.4
4r	62.9	56.4
4s	68.3	40.6
4t	80.6	47.8
4u	76.9	35.5
4v	87.3	14.5
Formononetin	26.4	>150
Gefitinib	91.5	6.2
Lapatinib	94.2	5.6

Biological studies

In order to screen out the optimal active compounds from all synthesized formononetin derivatives, a comparative study was carried out to evaluated their *in vitro* EGFR inhibition activities. As shown in Table 2, we clearly found that most of the tested

Table 3 *In vitro* cell proliferation of compounds **4a–4v**, formononetin and lapatinib against MCF-7, MDA-231 H460, H1650, L02 and VERO cell lines

Compound	IC$_{50}$ (μM)					
	MCF-7	MDA-231	H460	H1650	L02	VERO
4a	23.7 ± 1.87	15.1 ± 4.13	21.5 ± 2.04	11.9 ± 1.18	43.5 ± 3.64	25.3 ± 1.74
4b	24.5 ± 1.98	20.7 ± 1.62	18.5 ± 2.33	38.6 ± 3.56	>100	>100
4c	42.6 ± 0.25	33.6 ± 1.83	16.2 ± 2.05	17.8 ± 2.13	>100	>100
4d	21.5 ± 0.91	18.3 ± 1.03	16.5 ± 1.22	49.6 ± 3.65	65.8 ± 4.62	62.5 ± 2.01
4e	30.7 ± 1.42	27.8 ± 0.75	22.1 ± 2.87	33.4 ± 3.59	>100	>100
4f	23.9 ± 1.12	17.9 ± 2.25	24.3 ± 1.46	13.9 ± 1.44	>100	41.6 ± 2.48
4g	41.5 ± 2.01	19.5 ± 1.52	16.5 ± 5.49	12.9 ± 2.58	>100	>100
4h	17.8 ± 1.64	8.30 ± 1.23	8.02 ± 1.02	9.45 ± 1.08	>100	29.3 ± 1.94
4i	25.4 ± 1.73	16.3 ± 1.24	58.1 ± 3.54	19.7 ± 2.27	>100	57.9 ± 1.42
4j	25.7 ± 1.53	18.7 ± 1.02	19.6 ± 1.55	29.7 ± 2.59	>100	78.8 ± 2.23
4k	21.5 ± 0.63	23.2 ± 2.19	22.7 ± 2.28	10.8 ± 1.77	>100	36.5 ± 3.14
4l	21.1 ± 2.76	16.1 ± 2.75	16.3 ± 1.99	12.4 ± 1.68	>100	>100
4m	20.9 ± 2.24	9.35 ± 1.02	14.2 ± 1.69	22.5 ± 2.68	>100	>100
4n	19.5 ± 1.73	9.25 ± 1.05	18.2 ± 2.24	15.6 ± 2.07	>100	67.3 ± 1.52
4o	31.3 ± 1.93	33.8 ± 2.15	42.5 ± 6.42	10.1 ± 1.46	>100	>100
4p	24.6 ± 2.52	12.3 ± 1.49	15.5 ± 1.95	19.3 ± 2.04	>100	>100
4q	17.2 ± 1.93	15.4 ± 1.03	16.7 ± 2.49	8.79 ± 1.08	>100	>100
4r	15.9 ± 3.42	13.1 ± 1.84	24.6 ± 3.39	40.2 ± 3.88	>100	55.7 ± 2.05
4s	29.1 ± 1.27	10.1 ± 1.55	21.58 ± 2.09	15.3 ± 2.31	>100	>100
4t	12.3 ± 1.11	8.42 ± 1.21	18.6 ± 2.23	24.3 ± 1.89	>100	>100
4u	25.9 ± 1.94	13.2 ± 4.02	14.3 ± 1.84	12.2 ± 1.45	>100	>100
4v	11.5 ± 1.52	5.44 ± 1.28	6.36 ± 1.55	7.26 ± 1.02	>100	95.2 ± 4.72
Formononetin	36.4 ± 3.01	26.6 ± 2.84	27.8 ± 2.22	29.5 ± 3.25	82.6 ± 5.73	89.5 ± 5.82
Gefitinib	13.5 ± 3.08	12.5 ± 2.13	3.02 ± 0.89	2.64 ± 0.98	35.2 ± 3.08	38.6 ± 2.56
Lapatinib	7.10 ± 2.81	2.48 ± 1.04	1.22 ± 0.35	1.64 ± 0.98	42.5 ± 2.59	35.6 ± 2.25

Then we further evaluated their anti-proliferation activities against four cancer cell lines, human breast cancer cells (MCF-7, MDA-MB-231), human lung carcinoma cells (H460, H1650), as well as two non-cancer cell lines, normal human liver cells (L02) and African green monkey kidney cell (VERO) by the cell based MTT assay. The results are summarized in Table 3 and expressed by the half maximal inhibitory concentration (IC$_{50}$) values. As shown in Table 3, all compounds showed good anti-proliferation activity against the cancer cells, and most of them even better than formononetin itself with the standard of IC$_{50}$ values. To be specific, most compounds showed better anti-proliferation activity against MDA-MB-231 than MCF-7, which might because of the high expression of EGFR in the former. For MDA-MB-231 cell line, **4h** (IC$_{50}$ = 8.30 ± 1.23), **4m** (IC$_{50}$ = 9.35 ± 1.02 μM), **4n** (IC$_{50}$ = 9.25 ± 1.05 μM), **4t** (IC$_{50}$ = 8.42 ± 1.21 μM) and **4v** (IC$_{50}$ = 5.44 ± 1.28 μM) showed relatively better anti-proliferation activities than other compounds and their inhibitory efficacy against MDA-MB-231 were double stronger than against MCF-7 cell line (**4h**, IC$_{50}$ =
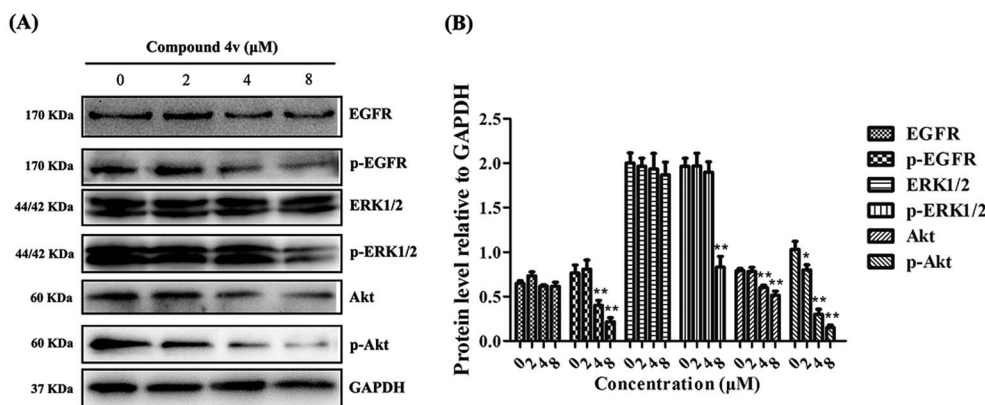

Fig. 3 The effects of **4v** on phosphorylation of EGFR and intracellular kinases in MDA-MB-231 cells. (A) Representative image of immunoblot analysis of EGFR signaling in MDA-MB-231 cells treated with **4v**. (B) Relative band intensity was determined by Image J software. GAPDH served as a loading control. Images are representative of three independent experiments. Data are means ± S.E.M. from three independent experiments (*$P < 0.05$; **$P < 0.01$).

17.8 ± 1.64 μM, **4m**, IC$_{50}$ = 20.9 ± 2.24 μM, **4n**, IC$_{50}$ = 19.5 ± 1.73 μM, **4t**, IC$_{50}$ = 12.3 ± 1.11 μM and **4v**, IC$_{50}$ = 11.5 ± 1.52 μM). Combined with the data of two human lung cancer cell lines, we clearly found that **4h** and **4v** showed much stronger inhibition effect than others, especially for **4v** (MCF-7, IC$_{50}$ = 11.5 ± 1.52 μM, MDA-MB-231, IC$_{50}$ = 5.44 ± 1.28 μM, H460, IC$_{50}$ = 6.36 ± 1.55 μM, H1650, IC$_{50}$ = 7.26 ± 1.02 μM), which effect is almost comparable to that of lapatinib (MCF-7, IC$_{50}$ = 7.1 ± 2.81 μM, MDA-MB-231, IC$_{50}$ = 2.48 ± 1.04 μM, H460, IC$_{50}$ = 1.22 ± 0.35 μM, H1650, IC$_{50}$ = 1.64 ± 0.98 μM) and much better than the inhibitory effect

of gefitinib against breast cancer cell lines (MCF-7, IC$_{50}$ = 13.5 ± 3.08 μM, MDA-MB-231, IC$_{50}$ = 12.5 ± 2.13 μM). Generally speaking, for comprehensive consideration anti-proliferation activities and the impact on log P (Table S2, ESI†), **4v** possessing 4-benzyloxy can be considered the optimal one in all newly synthetic compounds, and appeared to be a more efficient inhibitor of MDA-MB-231 cell viability (IC$_{50}$ = 5.44 ± 1.28 μM) when compared with formononetin (IC$_{50}$ = 26.6 ± 2.84 μM).

EGFR activation has been associated with multiple biological processes in cancer progression, such as cell proliferation,
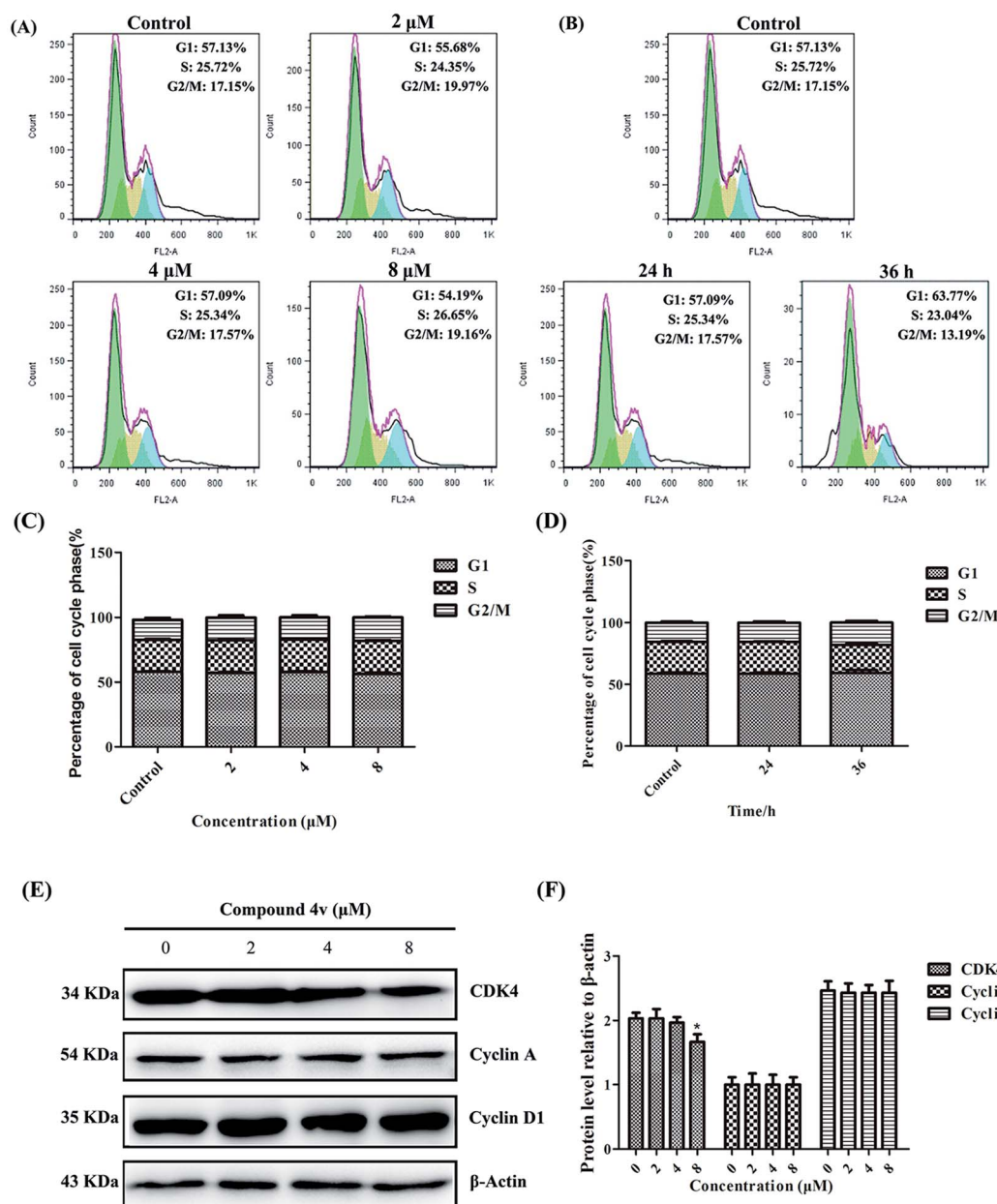
Fig. 4 The effects of **4v** on cell cycle distribution in MDA-MB-231 cells. (A) Cell cycle analysis of MDA-MB-231 cells treated with different concentrations of **4v**. (B) Cell cycle analysis of MDA-MB-231 cells treated with **4v** for different time (G1 phase, green; S phase, yellow and G2/M phase, blue). (C) Statistic analysis of dose-dependent assay. (D) Statistic analysis of time-dependent assay. (E) Representative image of immunoblot analysis of cell cycle related proteins in MDA-MB-231 cells treated with **4v**. (F) Relative band intensity was determined by Image J software. β-Actin served as a loading control. Images are representative of three independent experiments. Data are means ± S.E.M. from three independent experiments (*P < 0.05; **P < 0.01).

migration and metastasis through different signaling pathways.[26] To investigate the effect of 4v on signal transduction mechanism, we performed immunoblot analysis of EGFR and its downstream signaling pathways: extracellular signal regulated kinase (ERK) and Akt. As shown in Fig. 3, MDA-MB-231 cells that express high EGFR were treated with increasing concentrations of 4v and demonstrated a dose-dependent decrease in phosphorylation of EGFR, ERK and Akt.

To further substantiate the anti-proliferative effect of 4v on MDA-MB-231 cells, we evaluated its impact on the cell cycle arrest. As illustrated in Fig. 4A–D, 4v treated cells demonstrated no obvious cell cycle arrest versus the control groups. Then, we performed immunoblot analysis of cell cycle related proteins, Cyclin A, Cyclin D1 and CDK4. And the results shown in Fig. 4E and F indicated that the expression of the cell cycle related proteins in MDA-MB-231 cells did not increase after treated with compound 4v.

The transmembrane potential ($\Delta\Psi_m$) is an important parameter for mitochondrial functionality and its dissipation means the involvement of mitochondria in early apoptosis.[27] As shown in Fig. 5, microscopy revealed that in untreated MDA-MB-231 cells, well-polarized mitochondria were marked by red fluorescent staining. After treated with 2 or 4 μM of 4v, this pattern was replaced by green fluorescence in MDA-MB-231 cells. CCCP was used as the positive control here. Additionally, flow cytometry results also showed that untreated cells with well-polarized, red-emitting mitochondria localized in the upper region of the plot. Cells exposed to 4v for 12 hours underwent a progressive loss of red fluorescence, indicated by a downward in 4v treated groups. The ratio of cells with high membrane potential decreased from 85.2% to 80.8% after exposed to 2 μM 4v for 12 hours and even decreased to 56.8% in 4 μM 4v treated group. Likewise, the loss of mitochondrial potential in MDA-MB-231 cells caused by 4v also showed time-dependent manner.

Based on the above results, we also evaluated the apoptotic populations of MDA-MB-231 cells treated with 4v using flow cytometry analysis. As shown in Fig. 6A, cells treated with increasing concentrations of 4v and demonstrated a dose-dependent increase in apoptotic populations. In addition, cells treated with 4v for increasing time also demonstrated a time-dependent manner in apoptotic populations and
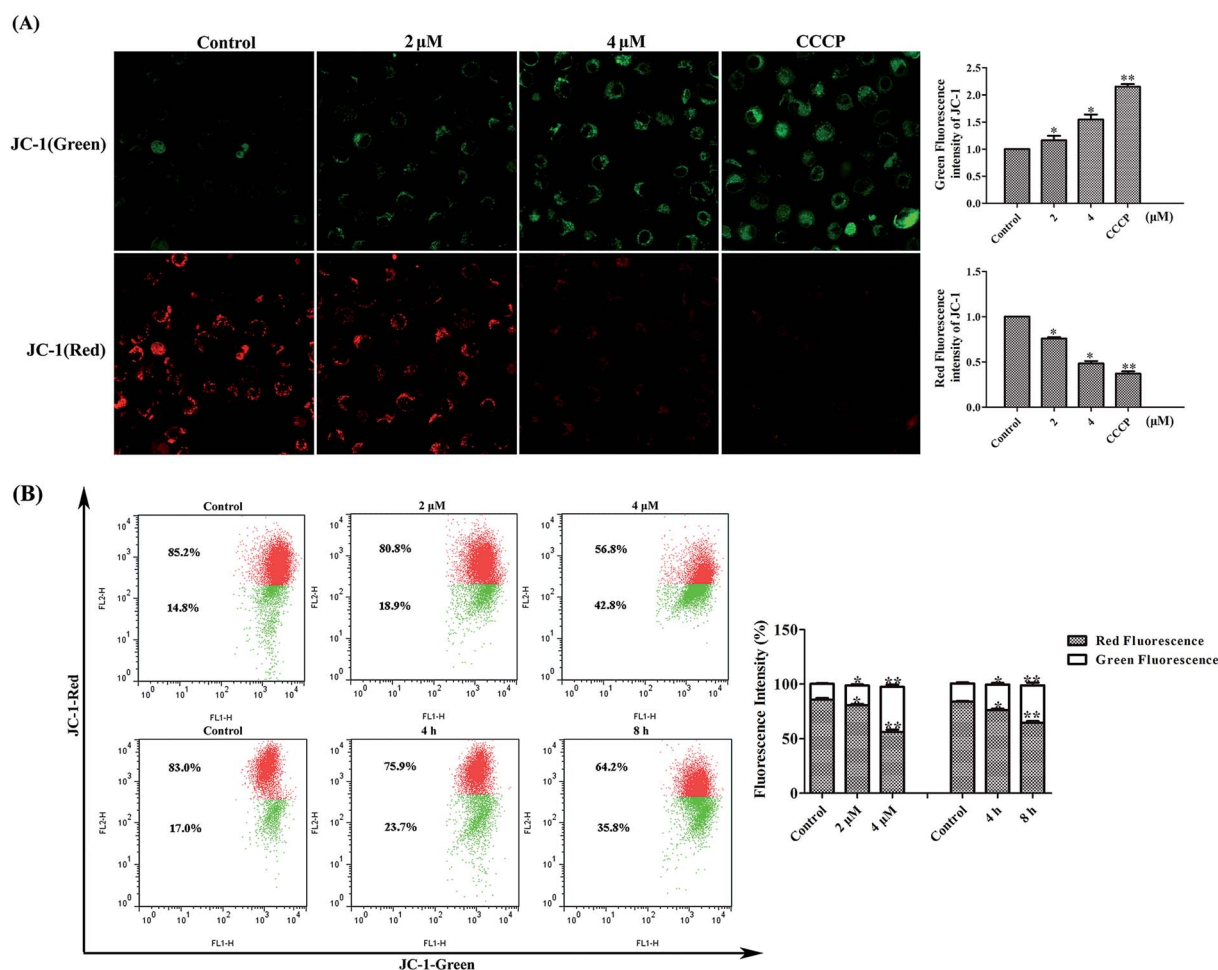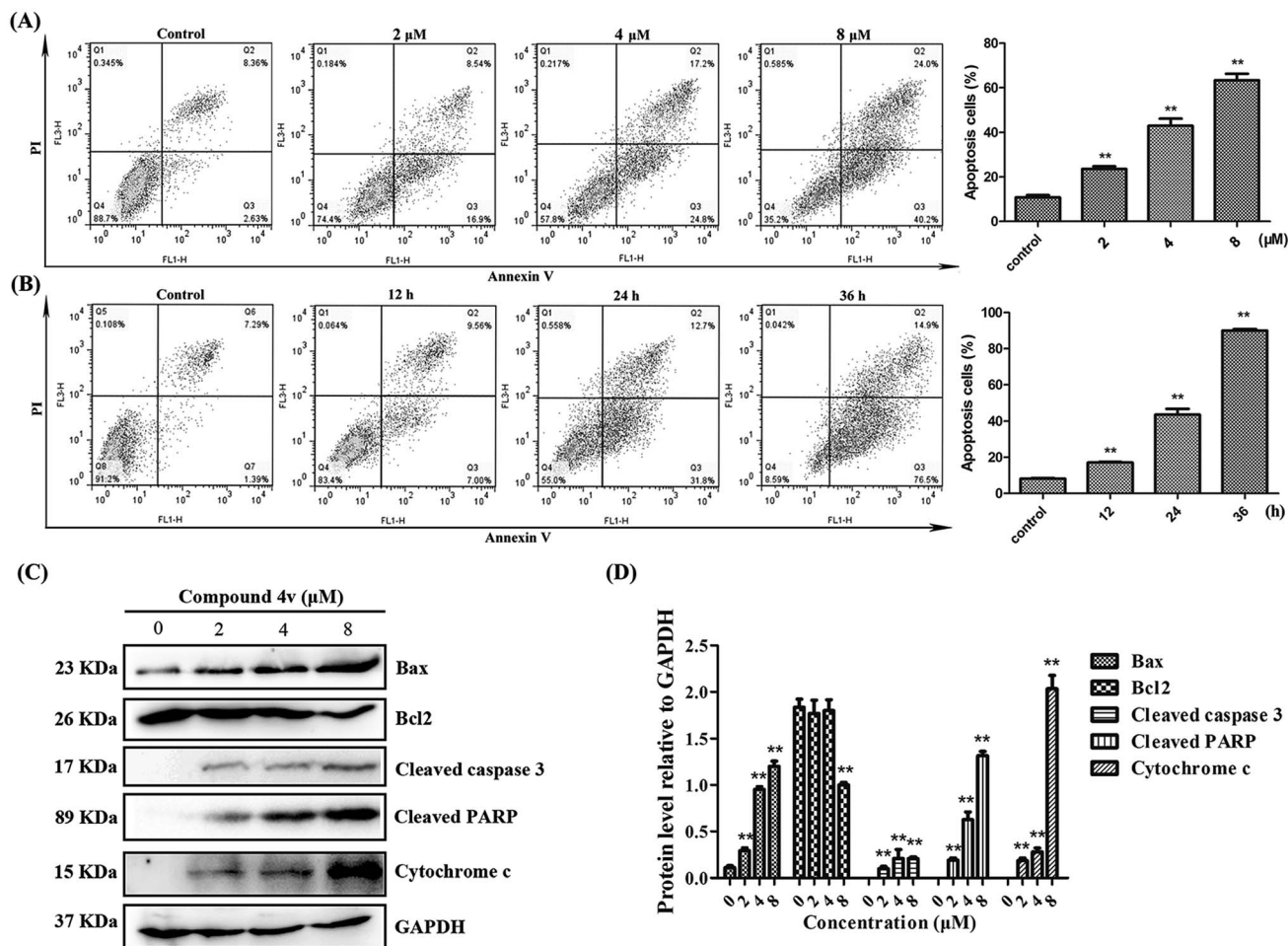

Fig. 5 4v decreased the mitochondrial membrane potential of MDA-MB-231 cells. (A) Cytofluorimetric analysis of mitochondrial membrane potential ($\Delta\Psi_m$) by JC-1 staining. (B) Flow cytometry analysis of MDA-MB-231 cells with high $\Delta\Psi_m$ (%) by JC-1 staining. Each point represents the mean ± S.E.M. from three replicates (*P < 0.05, **P < 0.01).

Fig. 6   The effects of **4v** on cell apoptosis in MDA–MB-231 cells. (A) Annexin V/PI double staining and cytometry analysis of **4v**-induced apoptosis in a dose-dependent manner. (B) Annexin V/PI double staining and cytometry analysis of **4v**-induced apoptosis in a time-dependent manner. (C) Western blot analyses of apoptosis-related proteins (Bax, Bcl2, cleaved caspase 3, cleaved PARP and cytochrome c) separated by SDS–PAGE. (D) Relative band intensity was determined by Image J software. GAPDH served as a loading control. Images are representative of three independent experiments. Data are means ± S.E.M. from three independent experiments (*$P < 0.05$; **$P < 0.01$).

a significant high percentage (approximately 90.4%) of apoptotic cells were observed in 36 hours-treated cells compared to vehicle control (Fig. 6B). This observation was further substantiated by concomitant increased expression of pro-apoptotic proteins, Bax, cytochrome c, cleaved caspase-3, cleaved PARP and decreased expression of anti-apoptotic Bcl2 after exposure to **4v** (Fig. 6C).

Tumor cell migration has been identified as one hallmark of malignant tumor progression, particularly for the establishment of lethal secondary metastases at distant organs. To investigate whether **4v** could inhibit the migratory capacity of MDA-MB-231 cells, the conventional *in vitro* wound healing assay was also conducted. As shown in Fig. 7A and B, the control group cells gradually occupied the cell-free space within the channel over time and the cells almost fill the channel after 48 hours. Whereas, cells migration capacity of **4v**-treated group was greatly inhibited and the inhibition was dose-dependent. The Wnt signaling pathway is crucial for multiple cellular processes including cell proliferation and migration. Once

activated, β-catenin disassembles from complex comprised of Axin, APC and GSK3β and translocates into nuclear. Then it interacts with TCF4 which promotes the downstream target gene transcription. On the basis of the wound healing assay, we subsequently investigated the influence of **4v** on Wnt signaling pathway in MDA-MB-231 cells. Western bolt analysis results shown in Fig. 7C indicated that treatment of MDA-MB-231 cells with **4v** resulted in the decrease expression of β-catenin and the increase expression of Axin-2 in dose-dependent manners. These results collectively suggested that **4v** might inhibit migration of MDA-MB-231 cells *via* Wnt signaling pathway.

To evaluate the anti-tumor effects of **4v** *in vivo*, we subcutaneously inoculated MDA-MB-231 cells in to the right flank of female nude mice. Two weeks later, all the mice got visible tumors. The mice were randomized into 3 groups, vehicle (olive oil), **4v** (5 mg kg⁻¹) and positive control (gefitinib, 5 mg kg⁻¹; lapatinib, 5 mg kg⁻¹). As shown in Fig. 8A, the administration of **4v** greatly inhibited the tumor growth compared with the vehicle group and the inhibition effect was similar to that of
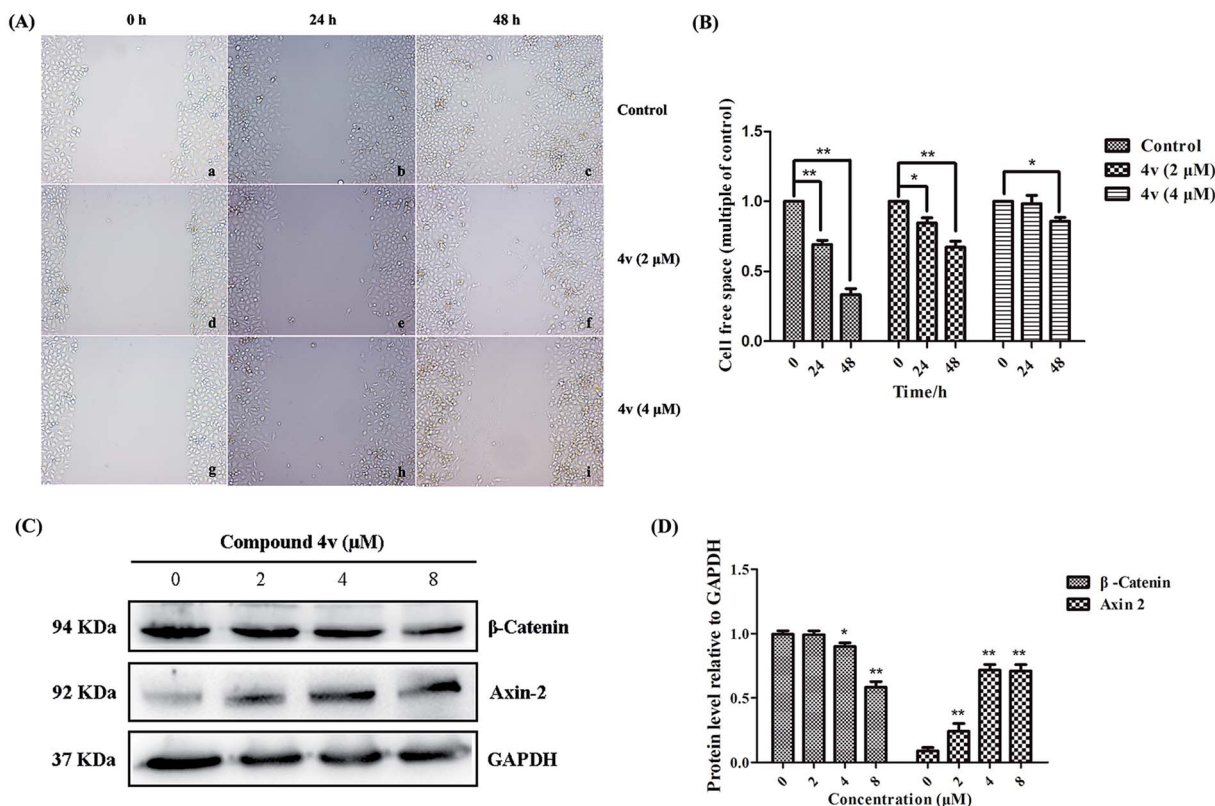
Fig. 7 The effects of **4v** on cell migration in MDA-MB-231 cells. (A) Cell migration was detected by the wound scrape assay. Representative images of cell migration in the wound scrape model at 0, 24 and 48 hours are shown. (B) Statistical analysis of the wound scrape assay. (C) Western blot analyses of Wnt signaling pathway proteins (β-catenin and Axin-2) separated by SDS-PAGE. (D) Relative band intensity was determined by Image J software. GAPDH served as a loading control. Images are representative of three independent experiments. The data represent the means ± S.E.M. of three independent experiments. *$P < 0.05$, **$P < 0.01$.

lapatinib, while the traditional EGFR inhibitor gefitinib showed extremely low therapeutic efficiency on MDA-MB-231 cells. After the last time of treatment on day 21, the average weight of tumors from **4v**-treated mice was nearly 2-fold less than the olive oil treated group (Fig. 8C). Meanwhile, **4v** has no significant influence on the body weight of the mice (Fig. 8B).

Experimental

General information and materials

Formononetin (purity ≥ 99%), ethyl bromoacetate, hydrazine hydrate, a series of benzaldehyde with different substituents, acetic acid, acetone, ethanol, *etc.* According to experimental conditions, all reagents used were of analytical reagent grade (AR) except ethanol which was purified and purchased from Nanjing Chemical Reagent Co. Ltd. (Nanjing, China). Gefitinib (purity ≥ 99%) and lapatinib (purity ≥ 99%) were purchased from J&K Scientific Ltd. (Shanghai, China). ^{1}H NMR and ^{13}C NMR spectra of all intermediate and final products were recorded on a DRX 600 spectrometer and DMSO-d6 as solvent. Chemical shifts (d) for ^{1}H NMR and ^{13}C NMR spectra were reported in ppm (d). The ESI-MS spectra were obtained on a Mariner Biospectrometry Workstation (ESI-TOF) mass spectrometer. Melting points of products were determined using

a XT4 MP Apparatus (Taike Corp., Beijing, China) and uncorrected. TLC was carried out on the glass-backed silica gel sheets (silica gel 60 Å GF254) and visualized in UV light (254 nm).

Cell culture reagents were purchased from Gibco Life Technology (Grand Island, NY, USA). MTT, PMSF, and RIPA lysis buffer (#P0013B) were purchased from Beyotime Institute of Biotechnology (Haimen, China). Cell Cycle Detection Kit and Annexin V-FITC/PI apoptosis detection kit were purchased from KeyGEN Biotech Co. Ltd (Nanjing, China). Mitochondrial membrane potential assay kit with JC-1 was purchased from Beyotime Biotech Co. Ltd (Haimen, China). BCA protein assay kit (#23227) was purchased from Pierce (Rockford, IL, USA). PVDF membranes were purchased from Biosharp (Hefei, China). Anti-Axin-2 (20540-1-AP) was purchased from Proteintech (Wuhan, China); anti-cleaved PARP-1 (#sc-56196) was purchased from Santa Cruz Biotechnology Inc. (Dallas, Texas, USA). Anti-EGFR (WL0682a), anti-ERK (WL01864), anti-p-ERK (WLP1512), anti-Akt (WL0003b), anti-p-Akt (WLP001a), anti-CDK4 (WL02143), anti-Cyclin A (WL01753), anti-Cyclin D1 (WL01435a), anti-β-Actin (WL0002c), anti-Bax (WL01637), anti-Bcl2 (WL01556), anti-cleaved caspase-3 (WL01992), anti-cytochrome c (WL01571) and anti-β-catenin (WL0962a) were purchased from Wanlei Biotech Co. Ltd (Shenyang, China). GAPDH antibody (#E1A7021) and secondary antibody (anti-
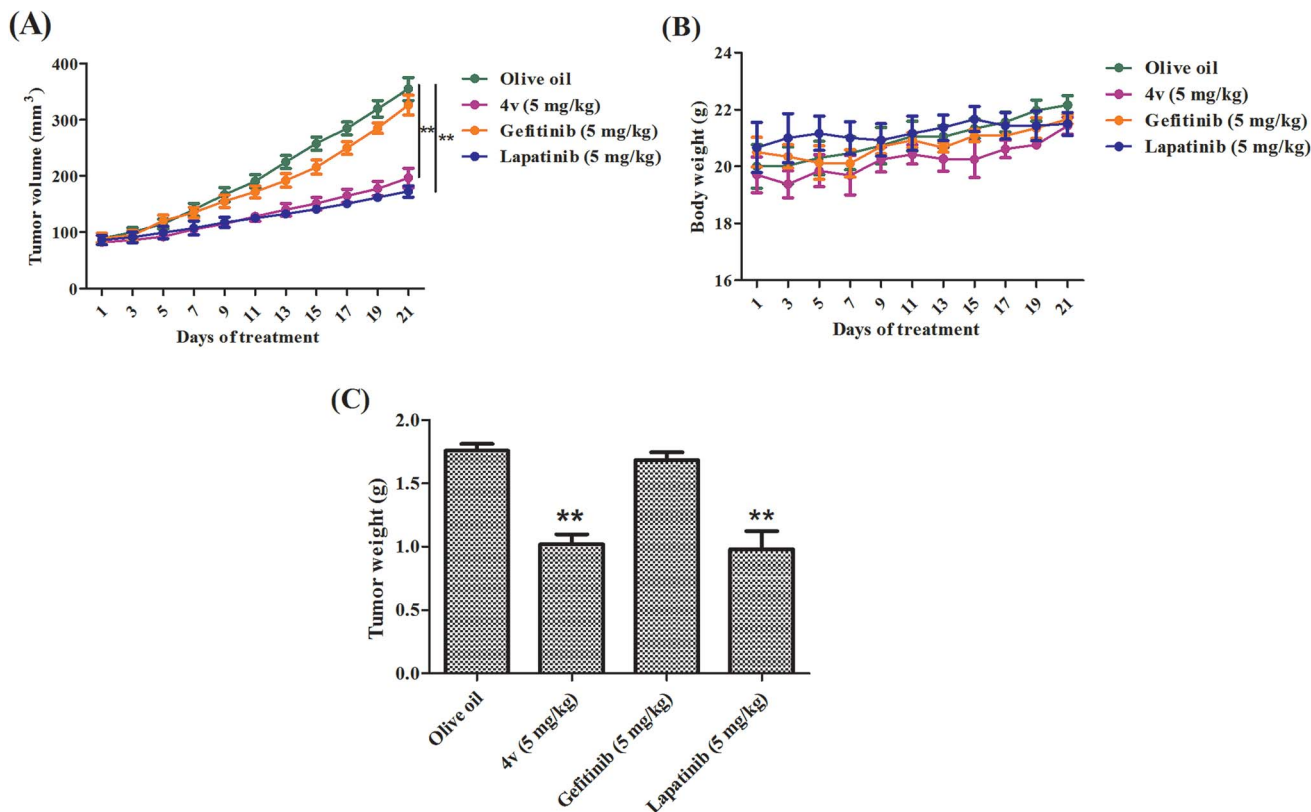
Fig. 8 **4v** suppresses tumor growth of MDA-MB-231 xenografts in nude mice. (A) Tumor volumes of the mice. (B) Body weight of the mice. (C) Tumor weight of mice. Data are the mean ± S.E.M. of 8 mice per group (*$P < 0.05$; **$P < 0.01$ *versus* vehicle (olive oil)).

mouse or anti-rabbit IgG) (#E1WP319 or #E1WP318) were purchased from Enogene (Nanjing, China). ECL Kit (#34077) were purchased from Thermo Scientific (USA).

General procedure for preparation of compound 2

A mixture of formononetin (0.04 mol, 11.44 g) and potassium carbonate (0.08 mol, 22.48 g) were stirred in acetone under the condition of reflux at 60 °C for 3 hours to get dissolved and clarified. Meanwhile, proportionable ethyl bromoacetate (0.04 mol, 4.9 g) was prepared which dissolved in appropriate acetone and added to the system dropwise to react another 10 hours. And then reaction system was filtered in hot to obtain filtrate. When the filtrate tended to be cooling, a large amount of compound **2** separated out and washed with petroleum ether, 1% sodium hydroxide and distilled water successively. The product was dried in the oven weighing 9.97 g (87%). White powder, yield 95%; mp: 188.5–189.3 °C; ^{1}H NMR (300 MHz, CDCl₃) δ 8.24 (d, $J = 8.9$ Hz, 1H), 7.92 (s, 1H), 7.53–7.46 (m, 2H), 7.03 (dd, $J = 8.9$, 2.4 Hz, 1H), 7.00–6.94 (m, 2H), 6.84 (d, $J = 2.4$ Hz, 1H), 4.73 (s, 2H), 4.31 (q, $J = 7.1$ Hz, 2H), 3.84 (s, 3H), 1.25 (dd, $J = 8.4$, 5.6 Hz, 3H). ESI-TOF, calcd for C₁₉H₁₆O₆ ([M + Na]⁺) 363.33, found 363.09. Anal. calcd for C₁₉H₁₆O₆: C, 67.06; H, 4.74; O, 28.21. Found: C, 66.87; H, 4.92; O, 28.29.

General procedure for preparation of compound 3

Compound **2** (0.025 mol, 8.85 g) was added to a clean round-bottom flask which contained 30–40 mL of ethanol. The reaction mixture was stirred under the condition of reflux at 80 °C. Hydrazine hydrate (0.075 mol, 3.9 g) was added and stirred for a further 10 hours with the reaction system getting clarified gradually. While stirring, the product was checked with TLC continually to choose the right point in time to stop the reaction. After the system temperature cooling to room temperature, the compound **3** which is white was isolated by filtration when precipitated. The product was dried in the oven weighing 7.45 g (84%). White powder, yield 87%; mp: 200.4–201.7 °C; ^{1}H NMR (300 MHz, DMSO) δ 9.32 (s, 1H), 7.78 (d, $J = 70.9$ Hz, 1H), 7.18 (d, $J = 8.2$ Hz, 2H), 7.07–6.68 (m, 3H), 6.43 (d, $J = 34.4$ Hz, 2H), 4.42 (s, 2H), 4.31 (s, 2H), 3.71 (s, 3H). ESI-TOF, calcd for C₁₇H₁₄N₂O₅ ([M + Na]⁺) 349.31, found 349.09. Anal. calcd for C₁₇H₁₄N₂O₅: C, 62.57; H, 4.32; N, 8.59; O, 24.52. Found: C, 61.94; H, 4.41; N, 8.66; O, 24.59.

General procedure for preparation of compounds 4a–4v

Compounds **4a–4v** were synthesized by reacting the compound **3** (0.0008 mol) with the different substituted ethyl benzaldehyde (0.0008 mol) in a Schiff base condensation reaction. The reaction was stirred at 80 °C for 8 hours in the presence of a bit of glacial acetic acid (4–8 drops) in ethanol. The compounds **4a–4v** were obtained by filtering after precipitation and all structure shown in Table 1.

(*Z*)-*N*′-Benzylidene-2-((3-(4-methoxyphenyl)-4-oxo-4*H*-chromen-7-yl)oxy)-acetohydrazide (4a). White powder, yield 75%; mp: 250.5–252.3 °C; 96.5% purity (HPLC); ^{1}H NMR (300 MHz, DMSO)

δ 11.60 (d, J = 7.3 Hz, 1H, –CH=N), 8.32–8.00 (m, 1H, Ar-H), 7.90–7.62 (m, 3H, N-NH, Ar-H), 7.44 (d, J = 3.6 Hz, 3H, Ar-H), 7.27–7.11 (m, 2H, Ar-H), 7.03 (t, J = 8.6 Hz, 1H, Ar-H), 6.85 (d, J = 8.1 Hz, 2H, Ar-H), 6.60–6.24 (m, 2H, Ar-H), 5.09–4.62 (m, 2H, –O–CH$_2$–), 3.72 (s, 3H, –OCH$_3$). ^{13}C NMR (75 MHz, DMSO) δ 169.43 (s, 14C), 164.73 (s, 18C), 159.64 (s, 11C), 158.04 (s, 6C), 157.08 (s, 16C), 148.40 (s, 9C), 144.35 (s, 19C), 134.56 (s, 20C), 134.32 (s, 23C), 130.68 (s, 2C), 130.46 (s, 4C), 129.32 (s, 21C, 25C), 129.29 (s, 22C, 24C), 127.62 (s, 13C), 127.40 (s, 3C), 126.75 (s, 8C), 119.13 (s, 15C), 114.32 (s, 1C, 5C), 105.83 (s, 12C), 102.47 (s, 10C), 66.88 (s, 17C), 55.45 (s, 7C). ESI-TOF, calcd for C$_{25}$H$_{20}$N$_2$O$_5$ ([M + Na]$^+$) 451.1372, found 451.1351. Anal. calcd for C$_{25}$H$_{20}$N$_2$O$_5$: C, 70.09; H, 4.71; N, 6.54; O, 18.67. Found: C, 69.58; H, 4.75; N, 6.61; O, 18.74.

(Z)-N′-(2-Fluorobenzylidene)-2-((3-(4-methoxyphenyl)-4-oxo-4H-chromen-7-yl)oxy)acetohydrazide (4b). White powder, yield 63%; mp: 245.7–247.1 °C; 95.3% purity (HPLC); ^{1}H NMR (300 MHz, DMSO) δ 11.71 (s, 1H, –CH=N), 8.62–8.19 (m, 1H, Ar-H), 7.91 (dt, J = 15.0, 7.6 Hz, 1H, Ar-H), 7.76 (s, 1H, N-NH), 7.55–7.39 (m, 1H, Ar-H), 7.35–7.22 (m, 2H, Ar-H), 7.21–7.13 (m, 2H, Ar-H), 7.02 (t, J = 9.1 Hz, 1H, Ar-H), 6.84 (d, J = 8.0 Hz, 2H, Ar-H), 6.62–6.22 (m, 2H, Ar-H), 5.15–4.60 (m, 2H, –O–CH$_2$–), 3.71 (s, 3H, –OCH$_3$). ^{13}C NMR (75 MHz, DMSO) δ 169.54 (s, 14C), 164.86 (s, 18C), 161.96 (s, 11C), 160.31 (s, 6C), 157.05 (s, 25C), 149.08 (s, 16C), 145.26 (s, 9C), 141.19 (s, 19C), 137.13 (s, 23C), 132.38 (d, J = 8.5 Hz, 21C), 126.90 (d, J = 15.3 Hz, 2C, 4C), 125.39 (s, 13C), 122.11 (s, 3C), 121.97 (s, 22C), 119.14 (s, 15C), 116.40 (s, 8C, 20C), 116.53 (s, 24C), 114.31 (s, 1C, 5C), 105.81 (s, 12C), 102.48 (s, 10C), 65.12 (s, 17C), 55.45 (s, 7C). ESI-TOF, calcd for C$_{25}$H$_{19}$FN$_2$O$_5$ ([M + Na]$^+$) 469.1278, found 469.1263. Anal. calcd for C$_{25}$H$_{19}$FN$_2$O$_5$: C, 67.26; H, 4.29; F, 4.26; N, 6.28; O, 17.92. Found: C, 67.14; H, 4.34; F, 4.31; N, 6.35; O, 18.02.

(Z)-N′-(3-Fluorobenzylidene)-2-((3-(4-methoxyphenyl)-4-oxo-4H-chromen-7-yl)oxy)acetohydrazide (4c). White powder, yield 73%; mp: 220.1–223.9 °C; 95.5% purity (HPLC); ^{1}H NMR (300 MHz, DMSO) δ 11.69 (s, 1H, –CH=N), 8.39–7.98 (m, 1H, Ar-H), 7.72 (s, 1H, N-NH), 7.63–7.37 (m, 3H, Ar-H), 7.31–7.11 (m, 3H, Ar-H), 7.08–6.92 (m, 1H, Ar-H), 6.84 (d, J = 7.9 Hz, 2H, Ar-H), 6.46 (t, J = 21.5 Hz, 2H, Ar-H), 5.15–4.60 (m, 2H, –O–CH$_2$–), 3.71 (s, 3H, –OCH$_3$). ESI-TOF, calcd for C$_{25}$H$_{19}$FN$_2$O$_5$ ([M + Na]$^+$) 469.1278, found 469.1263. Anal. calcd for C$_{25}$H$_{19}$FN$_2$O$_5$: C, 67.26; H, 4.29; F, 4.26; N, 6.28; O, 17.92. Found: C, 67.14; H, 4.34; F, 4.31; N, 6.35; O, 18.02.

(Z)-N′-(4-Fluorobenzylidene)-2-((3-(4-methoxyphenyl)-4-oxo-4H-chromen-7-yl)oxy)acetohydrazide (4d). White powder, yield 67%; mp: 261.9–263.1 °C; 96.6% purity (HPLC); ^{1}H NMR (300 MHz, DMSO) δ 11.60 (s, 1H, –CH=N), 8.35–7.96 (m, 1H, Ar-H), 7.89 (s, 1H, N-NH), 7.75 (dt, J = 10.2, 5.3 Hz, 2H, Ar-H), 7.25 (ddd, J = 21.7, 13.2, 6.1 Hz, 4H, Ar-H), 7.00 (s, 1H, Ar-H), 6.83 (s, 2H, Ar-H), 6.50 (d, J = 16.2 Hz, 2H, Ar-H), 5.1–4.55 (m, 2H, –O–CH$_2$–), 3.70 (s, 3H, –OCH$_3$). ESI-TOF, calcd for C$_{25}$H$_{19}$FN$_2$O$_5$ ([M + Na]$^+$) 469.1278, found 469.1263. Anal. calcd for C$_{25}$H$_{19}$FN$_2$O$_5$: C, 67.26; H, 4.29; F, 4.26; N, 6.28; O, 17.92. Found: C, 67.14; H, 4.34; F, 4.31; N, 6.35; O, 18.02.

(Z)-N′-(3,4-Difluorobenzylidene)-2-((3-(4-methoxyphenyl)-4-oxo-4H-chromen-7-yl)oxy)acetohydrazide (4e). White powder, yield 74%; mp: 238.5–239.8 °C; 96.3% purity (HPLC); ^{1}H NMR (300 MHz, DMSO) δ 11.70 (s, 1H, –CH=N), 8.34–7.94 (m, 1H, Ar-H), 7.90–7.64 (m, 2H, N-NH, Ar-H), 7.64–7.40 (m, 2H, Ar-H), 7.19 (d, J = 8.6 Hz, 2H, Ar-H), 7.01 (t, J = 8.6 Hz, 1H, Ar-H), 6.84 (d, J = 7.0 Hz, 2H, Ar-H), 6.45 (t, J = 20.6 Hz, 2H, Ar-H), 5.15–4.60 (m, 2H, –O–CH$_2$–), 3.71 (s, 3H, –OCH$_3$). ESI-TOF, calcd for C$_{25}$H$_{19}$F$_2$N$_2$O$_5$ ([M + Na]$^+$) 487.1184, found 487.1173. Anal. calcd for C$_{25}$H$_{19}$FN$_2$O$_5$: C, 64.66; H, 3.91; F, 8.18; N, 6.03; O, 17.22. Found: C, 64.58; H, 3.99; F, 8.23; N, 6.11; O, 17.31.

(Z)-N′-(2-Chlorobenzylidene)-2-((3-(4-methoxyphenyl)-4-oxo-4H-chromen-7-yl)oxy)acetohydrazide (4f). White powder, yield 75%; mp: 216.2–217.3 °C; 95.8% purity (HPLC); ^{1}H NMR (300 MHz, DMSO) δ 11.82 (d, J = 20.7 Hz, 1H, –CH=N), 8.78–8.32 (m, 1H, Ar-H), 8.00 (m, 2H, Ar-H), 7.78 (s, 1H, N-NH), 7.57–7.37 (m, 2H, Ar-H), 7.21 (dd, J = 7.0, 1.4 Hz, 2H, Ar-H), 7.09–6.95 (m, 1H, Ar-H), 6.86 (d, J = 8.5 Hz, 2H, Ar-H), 6.59–6.31 (m, 2H, Ar-H), 5.20–4.48 (m, 2H, –O–CH$_2$–), 3.73 (s, 3H, –OCH$_3$). ESI-TOF, calcd for C$_{25}$H$_{19}$ClN$_2$O$_5$ ([M + Na]$^+$) 485.0982, found 485.0974. Anal. calcd for C$_{25}$H$_{19}$ClN$_2$O$_5$: C, 64.87; H, 4.14; Cl, 7.66; N, 6.05; O, 17.28. Found: C, 64.69; H, 4.27; Cl, 7.74; N, 6.12; O, 17.32.

(Z)-N′-(3-Chlorobenzylidene)-2-((3-(4-methoxyphenyl)-4-oxo-4H-chromen-7-yl)oxy)acetohydrazide (4g). White powder, yield 78%; mp: 231.8–232.6 °C; 96.5% purity (HPLC); ^{1}H NMR (400 MHz, DMSO) δ 11.76 (s, 1H, –CH=N), 8.35–7.95 (m, 1H, Ar-H), 7.94 (s, 1H, N-NH), 7.85–7.72 (m, 1H, Ar-H), 7.68 (d, J = 3.2 Hz, 1H, Ar-H), 7.48 (dd, J = 13.8, 7.9 Hz, 2H, Ar-H), 7.21 (s, 2H, Ar-H), 7.04 (s, 1H, Ar-H), 6.87 (d, J = 22.1 Hz, 2H, Ar-H), 6.58–6.27 (m, 2H, Ar-H), 5.20–4.60 (m, 2H, –O–CH$_2$–), 3.71 (s, 3H, –OCH$_3$). ESI-TOF, calcd for C$_{25}$H$_{19}$ClN$_2$O$_5$ ([M + Na]$^+$) 485.0982, found 485.0974. Anal. calcd for C$_{25}$H$_{19}$ClN$_2$O$_5$: C, 64.87; H, 4.14; Cl, 7.66; N, 6.05; O, 17.28. Found: C, 64.69; H, 4.27; Cl, 7.74; N, 6.12; O, 17.32.

(Z)-N′-(4-Chlorobenzylidene)-2-((3-(4-methoxyphenyl)-4-oxo-4H-chromen-7-yl)oxy)acetohydrazide (4h). White powder, yield 59%; mp: 213.8–215.2 °C; 97.3% purity (HPLC); ^{1}H NMR (300 MHz, DMSO) δ 11.67 (s, 1H, –CH=N), 8.35–8.10 (m, 1H, Ar-H), 7.74 (dd, J = 8.5, 4.8 Hz, 2H, Ar-H), 7.51 (dd, J = 8.4, 5.0 Hz, 2H, Ar-H), 7.21 (d, J = 8.6 Hz, 2H, Ar-H), 7.08–6.75 (m, 7.5 Hz, 3H, Ar-H), 6.59–6.27 (m, 2H, Ar-H), 5.15–4.55 (m, 2H, –O–CH$_2$–), 3.72 (s, 3H, –OCH$_3$). ESI-TOF, calcd for C$_{25}$H$_{19}$ClN$_2$O$_5$ ([M + Na]$^+$) 485.0982, found 485.0979. Anal. calcd for C$_{25}$H$_{19}$ClN$_2$O$_5$: C, 64.87; H, 4.14; Cl, 7.66; N, 6.05; O, 17.28. Found: C, 64.69; H, 4.27; Cl, 7.74; N, 6.12; O, 17.32.

(Z)-N′-(2,3-Dichlorobenzylidene)-2-((3-(4-methoxyphenyl)-4-oxo-4H-chromen-7-yl)oxy)acetohydrazide (4i). White powder, yield 82%; mp: 214.2–215.6 °C; 96.5% purity (HPLC); ^{1}H NMR (300 MHz, DMSO) δ 11.89 (d, J = 20.9 Hz, 1H, –CH=N), 8.80–8.35 (m, 1H, Ar-H), 8.04–7.87 (m, 1H, Ar-H), 7.86–7.59 (m, 2H, N-NH, Ar-H), 7.43 (td, J = 7.9, 4.1 Hz, 1H, Ar-H), 7.19 (d, J = 8.4 Hz, 2H, Ar-H), 7.07–6.94 (m, 1H, Ar-H), 6.84 (d, J = 8.2 Hz, 2H, Ar-H), 6.46 (t, J = 23.2 Hz, 2H, Ar-H), 5.15–4.60 (m, 2H, –O–CH$_2$–), 3.71 (s, 3H, –OCH$_3$). ESI-TOF, calcd for C$_{25}$H$_{18}$Cl$_2$N$_2$O$_5$ ([M + Na]$^+$) 519.0593, found 519.0582. Anal. calcd for C$_{25}$H$_{18}$Cl$_2$N$_2$O$_5$: C, 60.38; H, 3.65; Cl, 14.26; N, 5.63; O, 16.08. Found: C, 60.29; H, 3.69; Cl, 14.30; N, 5.74; O, 16.15.

(Z)-N′-(2,6-Dichlorobenzylidene)-2-((3-(4-methoxyphenyl)-4-oxo-4H-chromen-7-yl)oxy)acetohydrazide (4j). White powder, yield 77%; mp: 181.6–182.7 °C; 95.6% purity (HPLC); ^{1}H NMR (300 MHz, DMSO) δ 11.86 (s, 1H, –CH=N), 8.55–8.22 (m, 1H, Ar-H),

7.95–7.60 (m, 1H, N-NH), 7.55 (d, J = 7.9 Hz, 2H, Ar-H), 7.48–7.35 (m, 1H, Ar-H), 7.18 (d, J = 8.0 Hz, 2H, Ar-H), 7.10–6.75 (m, 3H, Ar-H), 6.50 (d, J = 29.2 Hz, 2H, Ar-H), 5.05–4.60 (m, 2H, –O–CH$_2$–), 3.70 (s, 3H, –OCH$_3$). ^{13}C NMR (75 MHz, DMSO) δ 169.71 (s, 14C), 165.00 (s, 18C), 159.57 (s, 11C), 158.11 (s, 6C), 157.12 (s, 16C), 143.84 (s, 9C), 139.31 (s, 19C), 134.43 (s, 21C, 25C), 134.39 (s, 20C), 131.59 (s, 13C), 129.93 (s, 2C, 4C), 129.87 (s, 23C), 129.54 (s, 22C, 24C), 128.12 (s, 8C), 126.77 (s, 3C), 119.14 (s, 15C), 114.31 (s, 1C, 5C), 105.72 (s, 12C), 102.33 (s, 10C), 66.86 (s, 17C), 55.45 (s, 7C). ESI-TOF, calcd for C$_{25}$H$_{18}$Cl$_2$N$_2$O$_5$ ([M + Na]$^+$) 519.0593, found 519.0582. Anal. calcd for C$_{25}$H$_{18}$Cl$_2$N$_2$O$_5$: C, 60.38; H, 3.65; Cl, 14.26; N, 5.63; O, 16.08. Found: C, 60.29; H, 3.69; Cl, 14.30; N, 5.74; O, 16.15.

(*Z*)-*N*′-(3-Bromobenzylidene)-2-((3-(4-methoxyphenyl)-4-oxo-4*H*-chromen-7-yl)oxy)acetohydrazide (4k). White powder, yield 82%; mp: 224.0–225.2 °C; 97.8% purity (HPLC); ^{1}H NMR (300 MHz, DMSO) δ 11.69 (s, 1H, –CH=N), 8.30–7.95 (m, 1H, Ar-H), 7.90 (d, J = 9.7 Hz, 1H, Ar-H), 7.69 (d, J = 7.7 Hz, 1H, Ar-H), 7.59 (d, J = 6.6 Hz, 1H, Ar-H), 7.39 (dd, J = 14.5, 6.7 Hz, 1H, Ar-H), 7.19 (d, J = 8.4 Hz, 2H, Ar-H), 6.99 (d, J = 8.1 Hz, 1H, Ar-H), 6.84 (s, 2H, Ar-H), 6.56–6.22 (m, 2H, Ar-H), 5.15–4.59 (m, 2H, –O–CH$_2$–), 3.70 (s, 3H, –OCH$_3$). ESI-TOF, calcd for C$_{25}$H$_{19}$BrN$_2$O$_5$ ([M + Na]$^+$) 529.0477, found 529.0438. Anal. calcd for C$_{25}$H$_{19}$BrN$_2$O$_5$: C, 59.19; H, 3.77; Br, 15.75; N, 5.52; O, 15.77. Found: C, 59.10; H, 3.83; Br, 15.82; N, 5.59; O, 15.80.

(*Z*)-*N*′-(3-Hydroxybenzylidene)-2-((3-(4-methoxyphenyl)-4-oxo-4*H*-chromen-7-yl)oxy)acetohydrazide (4l). White powder, yield 82%; mp: 294.1–295.7 °C; 95.2% purity (HPLC); ^{1}H NMR (400 MHz, DMSO) δ 11.59 (s, 1H, –CH=N), 8.25–7.90 (m, 1H, Ar-H), 7.68 (s, 1H, N-NH), 7.28–6.95 (m, 6H, Ar-H), 6.83 (d, J = 8.1 Hz, 3H, Ar-H), 6.52 (d, J = 25.9 Hz, 2H, Ar-H), 5.15–4.60 (m, 2H, –O–CH$_2$–), 3.72 (s, 3H, –OCH$_3$). ^{13}C NMR (100 MHz, DMSO) δ 169.31 (s, 14C), 164.66 (s, 18C), 158.14 (s, 14C), 158.10 (s, 6C), 157.08 (s, 24C), 148.44 (s, 9C), 144.54 (s, 19C), 135.83 (s, 20C), 135.66 (s, 22C), 130.35 (s, 2C, 4C), 128.09 (s, 13C), 126.74 (s, 3C), 119.33 (s, 8C), 118.85 (s, 21C), 118.02 (s, 23C), 117.76 (s, 14C), 114.32 (s, 25C, 1C, 5C), 113.23 (s), 113.12 (s), 105.81 (s, 12C), 102.82 (s, 10C), 66.87 (s, 17C), 55.45 (s, 7C). ESI-TOF, calcd for C$_{25}$H$_{20}$N$_2$O$_6$ ([M + Na]$^+$) 467.1321, found 467.1314. Anal. calcd for C$_{25}$H$_{20}$N$_2$O$_6$: C, 67.56; H, 4.54; N, 6.30; O, 21.60. Found: C, 67.47; H, 4.61; N, 6.39; O, 21.65.

(*Z*)-*N*′-(4-Hydroxybenzylidene)-2-((3-(4-methoxyphenyl)-4-oxo-4*H*-chromen-7-yl)oxy)acetohydrazide (4m). White powder, yield 82%; mp: 248.3–249.5 °C; 95.3% purity (HPLC); ^{1}H NMR (300 MHz, DMSO) δ 11.38 (d, J = 8.6 Hz, 1H, –CH=N), 10.01 (s, 1H, –OH), 8.25–7.85 (m, 1H, Ar-H), 7.76 (s, 1H, N-NH), 7.51 (d, J = 8.4 Hz, 2H, Ar-H), 7.19 (dd, J = 8.8, 2.6 Hz, 2H, Ar-H), 7.01 (t, J = 8.5 Hz, 1H, Ar-H), 6.89–6.73 (m, 4H, Ar-H), 6.54–6.25 (m, 2H, Ar-H), 5.10–4.55 (m, 2H, –O–CH$_2$–), 3.70 (s, 3H, –OCH$_3$). ESI-TOF, calcd for C$_{25}$H$_{20}$N$_2$O$_6$ ([M + Na]$^+$) 467.1321, found 467.1314. Anal. calcd for C$_{25}$H$_{20}$N$_2$O$_6$: C, 67.56; H, 4.54; N, 6.30; O, 21.60. Found: C, 67.47; H, 4.61; N, 6.39; O, 21.65.

(*Z*)-*N*′-(4-Aminobenzylidene)-2-((3-(4-methoxyphenyl)-4-oxo-4*H*-chromen-7-yl)oxy)acetohydrazide (4n). Orange powder, yield 69%; mp: 247.6–248.3 °C; 95.4% purity (HPLC); ^{1}H NMR (300 MHz, DMSO) δ 11.23 (d, J = 5.6 Hz, 1H, –CH=N), 8.14–7.78 (m, 1H, Ar-H), 7.75 (s, 1H, N-NH), 7.34 (d, J = 8.5 Hz, 2H, Ar-H), 7.17 (dt, J =

14.1, 7.0 Hz, 2H, Ar-H), 7.00 (t, J = 8.3 Hz, 1H, Ar-H), 6.82 (t, J = 10.8 Hz, 2H, Ar-H), 6.56 (d, J = 8.0 Hz, 2H, Ar-H), 6.47–6.28 (m, 2H, Ar-H), 5.61 (d, J = 9.2 Hz, 2H, –NH$_2$), 5.55–4.51 (m, 2H, –O–CH$_2$–), 3.70 (s, 3H, –OCH$_3$). ESI-TOF, calcd for C$_{25}$H$_{21}$N$_3$O$_5$ ([M + Na]$^+$) 466.1481, found 466.1473. Anal. calcd for C$_{25}$H$_{21}$N$_3$O$_5$: C, 67.71; H, 4.77; N, 9.48; O, 18.04. Found: C, 67.65; H, 4.82; N, 9.53; O, 18.14.

(*Z*)-2-((3-(4-Methoxyphenyl)-4-oxo-4*H*-chromen-7-yl)oxy)-*N*′-(2-(trifluoromethyl)benzylidene)acetohydrazide (4o). White powder, yield 73%; mp: 203.1–204.5 °C; 96.7% purity (HPLC); ^{1}H NMR (300 MHz, DMSO) δ 11.90 (d, J = 35.0 Hz, 1H, –CH=N), 8.75–8.32 (m, 1H, Ar-H), 8.19 (dd, J = 16.1, 7.6 Hz, 1H, Ar-H), 7.85–7.52 (m, 4H, N-NH, Ar-H), 7.19 (d, J = 7.3 Hz, 2H, Ar-H), 7.09–6.91 (m, 1H, Ar-H), 6.84 (d, J = 7.5 Hz, 2H, Ar-H), 6.62–6.22 (m, 2H, Ar-H), 5.21–4.60 (m, 2H, –O–CH$_2$–), 3.70 (s, 3H, –OCH$_3$). ESI-TOF, calcd for C$_{26}$H$_{19}$F$_3$N$_2$O$_5$ ([M + Na]$^+$) 519.1246, found 519.1209. Anal. calcd for C$_{26}$H$_{19}$F$_3$N$_2$O$_5$: C, 62.90; H, 3.86; F, 11.48; N, 5.64; O, 16.11. Found: C, 62.82; H, 3.94; F, 11.53; N, 5.72; O, 16.24.

(*Z*)-2-((3-(4-Methoxyphenyl)-4-oxo-4*H*-chromen-7-yl)oxy)-*N*′-(4-(trifluoromethyl)benzylidene)acetohydrazide (4p). White powder, yield 68%; mp: 176.7–178.2 °C; 97.5% purity (HPLC); ^{1}H NMR (300 MHz, DMSO) δ 11.79 (s, 1H, –CH=N), 8.43–8.05 (m, 1H, Ar-H), 7.92 (d, J = 8.1 Hz, 2H, Ar-H), 7.78 (t, J = 7.2 Hz, 3H, N-NH, Ar-H), 7.19 (dd, J = 8.7, 2.1 Hz, 2H, Ar-H), 7.02 (t, J = 8.7 Hz, 1H, Ar-H), 6.84 (d, J = 8.3 Hz, 2H, Ar-H), 6.61–6.29 (m, 2H, Ar-H), 5.17–4.61 (m, 2H, –O–CH$_2$–), 3.71 (s, 3H, –OCH$_3$). ^{13}C NMR (75 MHz, DMSO) δ 169.73 (s, 14C), 165.08 (s, 18C), 159.79–159.10 (m, 11C), 158.05 (s, 6C), 157.08 (s, 16C), 146.63 (s, 9C), 142.67 (s, 19C), 138.56 (s, 20C), 138.39 (s, 23C), 130.18 (s, 2C, 4C), 128.20 (s, 21C, 25C), 128.01 (s, 13C), 126.74 (s, 22C, 24C), 126.16 (d, J = 4.7 Hz, 3C), 125.46 (s, C̲F$_3$), 123.66 (s, 8C), 119.13 (s, 15C), 114.31 (s, 1C, 5C), 105.79 (s, 12C), 102.54 (s, 10C), 66.84 (s, 17C), 55.44 (s, 7C). ESI-TOF, calcd for C$_{26}$H$_{19}$F$_3$N$_2$O$_5$ ([M + Na]$^+$) 519.1246, found 519.1209. Anal. calcd for C$_{26}$H$_{19}$F$_3$N$_2$O$_5$: C, 62.90; H, 3.86; F, 11.48; N, 5.64; O, 16.11. Found: C, 62.82; H, 3.94; F, 11.53; N, 5.72; O, 16.24.

(*Z*)-2-((3-(4-Methoxyphenyl)-4-oxo-4*H*-chromen-7-yl)oxy)-*N*′-(4-methylbenzylidene)acetohydrazide (4q). White powder, yield 62%; mp: 202.1–203.3 °C; 96.2% purity (HPLC); ^{1}H NMR (300 MHz, DMSO) δ 11.52 (d, J = 6.4 Hz, 1H, –CH=N), 8.32–7.9 (m, 1H, Ar-H), 7.74 (s, 1H, N-NH), 7.58 (d, J = 7.8 Hz, 2H, Ar-H), 7.35–7.10 (m, 4H, Ar-H), 7.01 (t, J = 8.6 Hz, 1H, Ar-H), 6.84 (d, J = 7.6 Hz, 2H, Ar-H), 6.45 (dd, J = 28.6, 17.3 Hz, 2H, Ar-H), 5.17–4.51 (m, 2H, –O–CH$_2$–), 3.71 (s, 3H, –OCH$_3$), 2.32 (s, 3H, –CH$_3$). ESI-TOF, calcd for C$_{26}$H$_{22}$N$_2$O$_5$ ([M + Na]$^+$) 465.1529, found 465.1513. Anal. calcd for C$_{26}$H$_{22}$N$_2$O$_5$: C, 70.58; H, 5.01; N, 6.33; O, 18.08. Found: C, 70.14; H, 5.16; N, 6.42; O, 18.14.

(*Z*)-*N*′-(2-Methoxybenzylidene)-2-((3-(4-methoxyphenyl)-4-oxo-4*H*-chromen-7-yl)oxy)acetohydrazide (4r). White powder, yield 86%; mp: 218.5–219.9 °C; 97.1% purity (HPLC); ^{1}H NMR (400 MHz, DMSO) δ 11.62 (d, J = 17.4 Hz, 1H, –CH=N), 8.71–8.32 (m, 1H, Ar-H), 7.84 (ddd, J = 16.7, 7.7, 1.5 Hz, 2H, N-NH, Ar-H), 7.47–7.34 (m, 1H, Ar-H), 7.21 (dd, J = 8.8, 2.4 Hz, 2H, Ar-H), 7.09 (t, J = 9.1 Hz, 1H, Ar-H), 7.02 (dt, J = 10.7, 8.2 Hz, 2H, Ar-H), 6.86 (d, J = 8.0 Hz, 2H, Ar-H), 6.60–6.27 (m, 2H, Ar-H), 5.15–4.55 (m, 2H, –O–CH$_2$–), 3.86 (d, J = 3.2 Hz, 3H, –OCH$_3$), 3.72 (s, 3H, –OCH$_3$). ESI-TOF, calcd for C$_{26}$H$_{22}$N$_2$O$_6$ ([M + Na]$^+$) 481.1478, found 481.1463.

Anal. calcd for $C_{26}H_{22}N_2O_6$: C, 68.11; H, 4.84; N, 6.11; O, 20.94. Found: C, 68.02; H, 4.92; N, 6.23; O, 20.98.

(Z)-N′-(4-Methoxybenzylidene)-2-((3-(4-methoxyphenyl)-4-oxo-4H-chromen-7-yl)oxy)acetohydrazide (4s). White powder, yield 75%; mp: 193.5–194.5 °C; 95.6% purity (HPLC); ^{1}H NMR (400 MHz, DMSO) δ 11.52 (s, 1H, –CH=N), 8.29–7.95 (m, 1H, Ar-H), 7.75–7.56 (m, 2H, Ar-H), 7.21 (d, J = 7.5 Hz, 2H, Ar-H), 7.01 (dd, J = 8.7, 6.8 Hz, 3H, Ar-H), 6.85 (s, 2H), 6.63–6.22 (m, 2H, Ar-H), 5.12–4.59 (m, 2H, –O–CH$_2$–), 3.80 (d, J = 2.8 Hz, 3H, –OCH$_3$), 3.72 (s, 3H, –OCH$_3$). ESI-TOF, calcd for $C_{26}H_{22}N_2O_6$ ([M + Na]$^+$) 481.1478, found 481.1463. Anal. calcd for $C_{26}H_{22}N_2O_6$: C, 68.11; H, 4.84; N, 6.11; O, 20.94. Found: C, 68.02; H, 4.92; N, 6.23; O, 20.98.

(Z)-N′-(3,4-Dimethoxybenzylidene)-2-((3-(4-methoxyphenyl)-4-oxo-4H-chromen-7-yl)oxy)acetohydrazide (4t). White powder, yield 63%; mp: 140.7–141.8 °C; 96.7% purity (HPLC); ^{1}H NMR (400 MHz, DMSO) δ 11.52 (d, J = 20.7 Hz, 1H, –CH=N), 8.28–7.90 (m, 1H, Ar-H), 7.73 (s, 1H, Ar-H), 7.32 (dd, J = 9.1, 1.6 Hz, 1H, Ar-H), 7.21 (dd, J = 8.4, 2.6 Hz, 3H, Ar-H), 7.03 (dd, J = 16.7, 8.3 Hz, 2H, Ar-H), 6.86 (d, J = 6.8 Hz, 2H, Ar-H), 6.59–6.31 (m, 2H, Ar-H), 5.18–4.60 (m, 2H, –O–CH$_2$–), 3.81 (dd, J = 8.5, 6.6 Hz, 6H, –OCH$_3$), 3.72 (s, 3H, –OCH$_3$). ESI-TOF, calcd for $C_{27}H_{24}N_2O_7$ ([M + Na]$^+$) 511.1584, found 511.1558. Anal. calcd for $C_{27}H_{24}N_2O_7$: C, 66.39; H, 4.95; N, 5.73; O, 22.93. Found: C, 66.24; H, 5.03; N, 5.86; O, 23.06.

(Z)-N′-(4-Isopropylbenzylidene)-2-((3-(4-methoxyphenyl)-4-oxo-4H-chromen-7-yl)oxy)acetohydrazide (4u). White powder, yield 86%; mp: 198.2–199.6 °C; 97.2% purity (HPLC); ^{1}H NMR (300 MHz, DMSO) δ 11.52 (d, J = 11.9 Hz, 1H, –CH=N), 8.31–7.95 (m, 1H, Ar-H), 7.75 (s, 1H, N-NH), 7.61 (d, J = 8.2 Hz, 2H, Ar-H), 7.30 (dd, J = 8.0, 5.1 Hz, 2H, Ar-H), 7.19 (dd, J = 8.8, 2.5 Hz, 2H, Ar-H), 7.02 (t, J = 8.6 Hz, 1H, Ar-H), 6.84 (d, J = 8.1 Hz, 2H, Ar-H), 6.56–6.30 (m, 2H, Ar-H), 5.12–4.55 (m, 2H, –O–CH$_2$–), 3.71 (s, 3H, –OCH$_3$), 2.90 (m, 1H, –CH(CH$_3$)$_2$), 1.20 (dd, J = 6.9, 1.8 Hz, 6H, –CH(CH$_3$)$_2$). ESI-TOF, calcd for $C_{28}H_{26}N_2O_5$ ([M + Na]$^+$) 493.1842, found 493.1837. Anal. calcd for $C_{28}H_{26}N_2O_5$: C, 71.48; H, 5.57; N, 5.95; O, 17.00. Found: C, 71.31; H, 5.62; N, 5.995; O, 17.12.

(Z)-N′-(4-(Benzyloxy)benzylidene)-2-((3-(4-methoxyphenyl)-4-oxo-4H-chromen-7-yl)oxy)acetohydrazide (4v). White powder, yield 69%; mp: 182.4–183.5 °C; 97.2% purity (HPLC); ^{1}H NMR (300 MHz, DMSO) δ 11.46 (d, J = 8.5 Hz, 1H, –CH=N), 8.30–7.90 (m, 1H, Ar-H), 7.80 (d, J = 8.4 Hz, 1H, N-NH), 7.63 (d, J = 8.3 Hz, 2H, Ar-H), 7.38 (ddd, J = 19.5, 13.1, 6.8 Hz, 5H, Ar-H), 7.19 (d, J = 8.0 Hz, 2H, Ar-H), 7.05 (dd, J = 15.8, 7.5 Hz, 3H, Ar-H), 6.85 (s, 2H, Ar-H), 6.58–6.22 (m, 2H, Ar-H), 5.14 (s, 2H, Ph-CH$_2$), 5.10–4.55 (m, 2H, –O–CH$_2$–), 3.70 (s, 3H, –OCH$_3$). ^{13}C NMR (75 MHz, DMSO) δ 169.17 (s, 14C), 164.43 (s, 18C), 160.48 (s, 11C), 160.26 (s, 23C), 148.21 (s, 6C), 144.14 (s, 16C), 137.21 (s, 9C), 129.24 (s, 19C), 128.99 (s, 27C), 128.94 (s, 2C, 4C, 21C, 25C), 128.42 (s, 29C, 31C), 128.25 (s, 13C), 127.31 (s, 28C, 32C), 127.23 (s, 31C), 115.62 (s, 20C, 3C), 114.32 (s, 1C, 5C, 22C, 24C), 105.80 (s, 8C, 12C), 102.86 (s, 15C), 102.45 (s, 10C), 69.81 (s, 26C), 66.89 (s, 17C), 55.45 (s, 7C). ESI-TOF, calcd for $C_{32}H_{26}N_2O_6$ ([M + Na]$^+$) 557.1791, found 557.1805. Anal. calcd for $C_{32}H_{26}N_2O_6$: C, 71.90; H, 4.90; N, 5.24; O, 17.96. Found: C, 71.83; H, 4.98; N, 5.31; O, 18.03.

Cell lines and culture conditions

The cell lines used in this study were MCF-7, MDA-MB-231, H460, H1650, L02 and VERO. They were obtained from State Key Laboratory of Pharmaceutical Biotechnology, Nanjing University. MCF-7, MDA-MB-231, L02 and VERO cells were maintained in DMEM/high glucose supplemented with 10% FBS, L-glutamine, and penicillin/streptomycin and incubated at 37 °C in humidified atmosphere containing 5% CO$_2$. H460 and H1650 cells were maintained in RPMI.1640 medium supplemented with 10% FBS and penicillin/streptomycin and incubated at 37 °C in humidified atmosphere containing 5% CO$_2$.

Animals feeding

Female nude mice (5–7 weeks old) were obtained from Model Animal Research Center of Nanjing University (Nanjing, China). Briefly, mice were fed with free access to pellet food and water in plastic cages at 21 ± 2 °C and kept on a 12 hours light–dark cycle. All animal procedures were performed in accordance with the Guidelines for Care and Use of Laboratory Animals of Nanjing University and approved by the Animal Ethics Committee of the Ministry of Science and Technology of China (2006). All efforts were made to minimize animal suffering and to reduce the number of animals used.

EGFR kinase phosphorylation assay

The assays were carried out as described previously.[3,28] Phosphorylation assays were performed in a final volume of 20 μL containing 8 mM MOPS (pH 7.0), 0.2 mM EDTA, 10 mM MnCl$_2$, 200 μM substrate peptide, 0.25 mM DTT, 0.1 mg mL^{-1} BSA, 10 ng of wild-type EGFR kinase (catalogue no. 40187, BPS Bioscience), 10 mM magnesium acetate, 100 μM γ-[^{32}P] ATP, and inhibitors or DMSO control (1.25% v/v). For IC$_{50}$ curves with the wild-type enzyme, the following concentrations of the compounds were tested in triplicate: 150, 100, 50, 25, 15, 10, 7.5, 5, and 2.5 nM. Reactions were started by the addition of the magnesium acetate/ATP mixture. After 30 minutes incubation at 30 °C, 5 μL of each reaction was spotted on phosphocellulose P81 paper (Whatman). The P81 paper was then washed 5 times with 50 mM phosphoric acid for 15 minutes, dried, and exposed to a phosphorimager screen (Storm, GE Healthcare), which was scanned and densitometrically analyzed the next day. The sequence of the substrate peptide was derived from phospholipase C-γ1. The IC$_{50}$ values were calculated using nonlinear regression with normalized dose response fit using Prism GraphPad software.

Anti-proliferation assay

The anti-proliferation activity of the prepared compounds against four cancer cell lines, MCF-7, MDA-MB-231, H460, H1650 and two normal cell lines, L02 and VERO were evaluated as described elsewhere.[29] Four kinds of cancer cell lines and two normal cell lines were plated in 96-well plates at the appropriate density (2.0×10^3 cells per well) with maintained in DMEM (or 1640 medium) with 10% FBS and cultivated for 12 hours at 37 °C, 5% CO$_2$ atmosphere. All cells treated with different

concentrations (0, 0.1, 1, 10 and 100 μM) of each compound with formononetin and lapatinib as positive references. After 24 hours, 20 μL PBS containing of MTT solution (2.5 mg mL^{-1}) was added to each well and incubated for a further 4 hours. Then 150 μL of DMSO was added to each well to dissolve purple crystal. The plates were shaken to ensure the completion solubility for 10 minutes at room temperature. The values of absorbance were recorded on ELISA reader (ELx800, BioTek, USA) at a wavelength of 570 nm. All experiments were performed in three replicate wells for each concentration of all compounds including formononetin, and all assay experiments were carried out three times. The IC$_{50}$ values defined as the concentrations that cause a 50% loss of cell viability were calculated by Origin 7.5 and exhibited in Table 3.

Apoptosis analysis by flow cytometry

Cell apoptosis assay of compound 4v for MDA-MB-231 cell was carried out by Annexin V/PI assays and monitored by flow cytometry. Briefly, 5 × 10^3 cells per well were seeded in 6-well plates for 12 hours and then treated with 4v (0, 2, 4 and 8 μM) for 24 hours or treated with 4 μM 4v for 0, 12, 24 and 36 hours. Next, cells were collected and washed twice with PBS and then centrifuged to obtain sedimentation. 500 μL 1× binding buffer (10 mM HEPES, PH 7.4, 140 mM NaOH, 2.5 mM CaCl$_2$) was added to each EP tube to make cells resuspended and stained with 5 μL of Annexin V-FITC and 5 μL of PI for 30 minutes at room temperature in the dark. Apoptotic cells were quantified using a BD Accuri C6 Flowjo Cytometer (BD, USA). Statistical analysis was done using Flowjo 7.6.1 software.

Mitochondrial membrane potential staining

JC-1 is an ideal fluorescent probe which is widely used in the detection of mitochondrial membrane potential ($\Delta\Psi_m$). According to the requirements, MDA-MB-231 cells were cultured in 6-well plates (5 × 10^3 cells per well) for 12 hours at 37 °C, 5% CO$_2$ atmosphere and then treated with compound 4v (0, 2 and 4 μM) for 12 hours and with positive control drug, CCCP in another well for 30 minutes at 37 °C. Cell in all wells were collected and rinsed with PBS. Then 500 μL JC-1 staining solution (5×) was added to each EP tube and incubated at 37 °C for 20 minutes. Finally, cells were washed twice with JC-1 staining solution (1×) and then resuspended to detect by BD Accuri C6 Flowjo Cytometer and Olympus confocal microscope, and data was analyzed using FV-10-ASW 1.7 viewer.

Cell cycle arrested analysis by flow cytometry

After incubation in 6-well plates (5 × 10^3 cells per well), MDA-MB-231 cells were treated with compound 4v (0, 2, 4 and 8 μM) for 24 hours or treated with 4 μM 4v for 0, 24 and 36 hours. After that, cells were collected and washed twice with PBS and then fixed in 70% ethanol at 4 °C for at least 2 hours. Next, cells were resuspended in PBS with 0.1 mg mL^{-1} RNase A and 5 mg mL^{-1} propidium iodide (PI) in the dark condition. The measure was performed by BD Accuri C6 Flowjo Cytometer (BD, USA). The date of cells in the G1, S and G2/M phases of the cell cycle were counted using the Flowjo 7.6.1 software excluding cell debris.

Wound-healing assay

MDA-MB-231 cells were seeded in a tissue culture 6-well plate at an initial density of 2 × 10^5 cells per cm^2 overnight. A micropipette tip was used to create a wound in the monolayer by scraping after cells seeding and incubation for 24 hours. Identical cell-free space was observed by phase-contrast microscopy (NIKON, Japan) and digital images were taken by cells at 0, 24 and 48 hours. Subsequently, the NIH Image J image analysis software was used to outline the wound areas and analysis quantifies the reduced cell-free space, $n = 3$.

Western blot analysis

Total proteins were extracted from MDA-MB-231 cells which were treated with compound 4v at different concentrations (0, 2, 4 and 8 μM). Cells obtained were lysed in RIPA lysis buffer containing protease inhibitor phenylmethanesulfonyl fluoride (PMSF, PMSF : RIPA = 1 : 100) on ice for 20–30 minutes. Protein content was measured using a Pierce BCA protein assay kit. Protein samples were separated by sodium dodecyl sulphate-polyacrylamide gel electrophoresis (SDS-PAGE) and then transferred onto polyvinylidene difluoride (PVDF) membranes which were blocked with 5% non-fat-milk for 1 hour. All membranes were separated and incubated with primary antibodies including EGFR (rabbit polyclonal IgG, 1 : 1000 dilution), p-EGFR (rabbit polyclonal IgG, 1 : 1000 dilution), ERK (rabbit polyclonal IgG, 1 : 500 dilution), p-ERK (rabbit polyclonal IgG, 1 : 500 dilution), Akt (rabbit polyclonal IgG, 1 : 500 dilution), p-Akt (rabbit polyclonal IgG, 1 : 500 dilution), GAPDH (rabbit polyclonal IgG, 1 : 1000 dilution), CDK4 (rabbit polyclonal IgG, 1 : 500 dilution), Cyclin A (rabbit polyclonal IgG, 1 : 500 dilution), Cyclin D1 (rabbit polyclonal IgG, 1 : 500 dilution), β-actin (rabbit polyclonal IgG, 1 : 500 dilution), Bax (rabbit polyclonal IgG, 1 : 500 dilution), Bcl2 (rabbit polyclonal IgG, 1 : 500 dilution), cleaved caspase-3 (rabbit polyclonal IgG, 1 : 500 dilution), cleaved-PARP (mouse monoclonal IgG, 1 : 600 dilution), cytochrome c (rabbit polyclonal IgG, 1 : 500 dilution), β-catenin (rabbit polyclonal IgG, 1 : 500 dilution) and Axin-2 (rabbit polyclonal IgG, 1 : 1000 dilution) at 4 °C shaking overnight. After the membrane was washed three times with tris-buffered saline buffer, HRP-conjugated secondary antibody (diluted 1 : 50 000) was used at room temperature. Detection was performed by an enhanced chemiluminescent reagent (Thermo Fisher Scientific, USA) according to the manufacturer's instructions. Bands were then recorded by a digital camera (Tanon 5200, Tanon, China). Finally, the results were analyzed with Image J Software (National Institutes of Health, BetheSEMa, Maryland, USA), and all the targeted protein were normalized to GAPDH or β-actin.

Transplantation of MDA-MB-231 cells into nude mice

Cultured MDA-MB-231 cells were washed with and resuspended in ice-cold PBS. Portions of the suspension (6 × 10^6 cells in 0.1 mL) were injected into the right flanks of female nu/nu mice. Two weeks after the injection, the mice bearing tumors (an

average size of 90 mm^3) were distributed into 3 groups ($n = 8$ mice per group) according to tumor volumes. **4v** (5 mg kg^{-1}) and lapatinib (5 mg kg^{-1}) were dissolved in olive oil and administered once every two days for 11 times by intraperitoneal injection. Vehicle (olive oil)-treated group was included as control. Body weight and tumor volumes were measured and recorded every two days. Long diameter (L) and short diameter (S) of a tumor were measured with a vernier caliper and the tumor volume was calculated using the following formula: $L \times (S)^2/2$. Twenty-one days after injection, the mice were killed and tumors were separated. Tumor weight was measured and tumor sections were fixed in paraformaldehyde. The rest of the sections were frozen in liquid nitrogen and stored at $-80\ ^\circ$C.

Data and statistical analysis

All experiments were repeated at least three times. Data are presented as mean ± S.E.M. and statistical comparisons between the treated and untreated groups were performed using one-way ANOVA using GraphPad PRISM5 (Graphpad Inc., La Jolla, USA). P-Values of <0.05 were considered statistically significant; P-values of <0.01 were considered statistically very significant.

Conclusion

In this study, a series of novel formononetin derivatives targeting EGFR kinase were designed, synthesized and evaluated for their potential anti-proliferation activities against human breast and lung cancer cell lines. Among them, compound **4v** (IC$_{50}$ = 14.5 nM) showed potent EGFR inhibitory activity which was almost comparable to that of gefitinib (IC$_{50}$ = 6.2 nM) and lapatinib (IC$_{50}$ = 5.6 nM). For *in vitro* anti-proliferation activities, **4v** exhibited potent inhibitory activity against MDA-MB-231 cell line (IC$_{50}$ = 5.44 ± 1.28 μM) which was also comparable to lapatinib (IC$_{50}$ = 2.48 ± 1.04 μM) but much better than gefitinib (IC$_{50}$ = 12.5 ± 2.13 μM) and formononetin (IC$_{50}$ = 26.6 ± 2.84 μM) itself. The structure–activity relationship (SAR) analyzed by molecular docking showing that **4v** could bind well to the active site of EGFR as lapatinib. Flow cytometry analysis and mitochondrial membrane potential staining results demonstrated that **4v** could effectively cause loss of mitochondrial membrane potential and then induce apoptosis on MDA-MB-231 cells, but had no significant influence on cell cycle distribution. Western blot results further confirmed that **4v** inhibited MDA-MB-231 cell proliferation by blocking EGFR downstream Ras/Raf/MEK/ERK signaling pathway and induced MDA-MB-231 cell apoptosis by regulating EGFR/PI3K/Akt/Bad pathway. In addition, **4v** could also effectively inhibit migration of MDA-MB-231 cells involving to Wnt signaling pathway. The preliminary *in vivo* anti-tumor results demonstrated the effectiveness of **4v** in tumor chemotherapy in mice and indicated its possibility as a new EGFR inhibitor in curing MDA-MB-231 malignant tumor.

Conflicts of interest

The authors declare no conflict of interest.

Abbreviations

CADD	Computer assist drug design
CCCP	Carbonylcyanidem-chlorophen-ylhydrazone
EGF	Epidermal growth factor
EGFR	Epidermal growth factor receptor
ESI-MS	Electrospray ionization-mass spectrometry
HER2	Human epidermal growth factor receptor-2
HEPES	4-(2-Hydroxyethyl)-1-piperazineethanesulfonic acid
MAPK	Mitogen-activated protein kinase
MTT	3-(4,5-Dimethylthiazol-2-yl)-2,5-diphenyltetrazolium bromide
NSCLC	Non-small-cell carcinoma
PARP	Poly-ADP ribose polymerase
PI	Propidium iodide
SAR	Structure–activity relationship
TLC	Thin layer chromatography
UV	Ultraviolet

Notes and references

1 A. Olayioye, R. M. Neve and N. E. Hynes, *EMBO J.*, 2000, **17**, 3159–3167.

2 I. Okamoto, *FEBS J.*, 2010, **277**, 309–315.

3 M. M. Hamed, S. S. Darwish, J. Herrmann, A. H. Abadi and M. Engel, *J. Med. Chem.*, 2017, **60**, 2853–2868.

4 Y. Yamanaka, H. Friess, M. Kobrin, M. Buchler, H. Beger and M. Korc, *Anticancer Res.*, 1992, **13**, 565–569.

5 J. M. Rae and M. E. Lippman, *Breast Cancer Res. Treat.*, 2004, **83**, 99–107.

6 R. E. Sobol, R. W. Astarita, C. Hofeditz, H. Masui, R. Fairshter, I. Royston and J. Mendelsohn, *J. Natl. Cancer Inst.*, 1987, **79**, 403–407.

7 S. Balakrishnan, S. Mukherjee, S. Das, F. A. Bhat, P. Raja Singh, C. R. Patra and J. Arunakaran, *Cell Biochem. Funct.*, 2017, **35**, 217–231.

8 K. Takasawa, A. Takasawa, M. Osanai, T. Aoyama, Y. Ono, T. Kono, Y. Hirohashi, M. Murata and N. Sawada, *Cancer Lett.*, 2017, **403**, 66–73.

9 A. Sgambato, F. Casaluce, P. Maione, A. Rossi, E. Rossi, A. Napolitano, G. Palazzlol, M. A. Bareschion, C. Schettino, P. C. Sacco, F. Ciadiello and C. Gridelli, *Curr. Med. Chem.*, 2012, **19**, 3337–3352.

10 K. Manupati, N. R. Dhoke, T. Debnath, R. Yeeravalli, K. Goguloth, S. Saeidpour, U. C. De, S. Debnath and A. Das, *FEBS J.*, 2017, **284**, 1830–1854.

11 M. J. Duffy, P. M. Mcgowan and J. Crown, *Int. J. Cancer*, 2012, **131**, 2471–2477.

12 D. Zhang, A. M. Tari, U. Akar, B. K. Arun, T. A. LaFortune, R. Nieves-Alicea, G. N. Hortobagyi and N. T. Ueno, *Mol. Cancer Ther.*, 2010, **9**, 3090–3099.

13 O. Lapčik, M. Hill, I. Černý, J. Lachman, N. Al-Maharik, H. Adlercreutz and R. Hampl, *Plant Sci.*, 1999, **148**, 111–119.

14 L. Hutabarat, H. Greenfield and M. Mulholland, *J. Chromatogr. A*, 2000, **886**, 55–63.

15 X. Y. Wu, H. Xu, Z. F. Wu, C. Chen, J. Y. Liu, G. N. Wu, X. Q. Yao, F. K. Liu, G. Li and L. Shen, *Oncotarget*, 2015, **6**, 44563–44578.

16 X. Yu, W. Wang and M. Yang, *Food Chem.*, 2007, **104**, 715–720.

17 T. Fukai, A. Marumo, K. Kaitou, T. Kanda, S. Terada and T. Nomura, *Life Sci.*, 2002, **71**, 1449–1463.

18 Y. Ungar, O. F. Osundahunsi and E. Shimoni, *J. Agric. Food Chem.*, 2003, **51**, 4394–4399.

19 S. Sato, J. Takeo, C. Aoyama and H. Kawahara, *Bioorg. Med. Chem.*, 2007, **15**, 3445–3449.

20 Z. N. Ji, W. Zhao, G. Liao, R. Choi, C. K. Lo, T. T. X. Dong and K. W. K. Tsim, *Gynecol. Endocrinol.*, 2006, **22**, 578–584.

21 S. Medjakovic and A. Jungbauer, *J. Steroid Biochem.*, 2008, **108**, 171–177.

22 Y. M. Jin, T. M. Xu, Y. H. Zhao, Y. C. Wang and M. H. Cui, *Tumor Biol.*, 2014, **35**, 2279–2284.

23 D. J. Fu, L. Zhang, J. Song, R. W. Mao, R. H. Zhao, Y. C. Liu, Y. H. Hou, J. H. Li, J. J. Yang, C. Y. Jin, P. Li, X. L. Zi, H. M. Liu, S. Y. Zhang and Y. B. Zhang, *Eur. J. Med. Chem.*, 2016, **127**, 87–99.

24 Y. Q. Li, F. Yang, L. Wang, Z. Cao, T. J. Han, Z. A. Duan, Z. Li and W. J. Zhao, *Eur. J. Med. Chem.*, 2016, **112**, 196–208.

25 J. Ren, H. J. Xu, H. Cheng, W. Q. Xin, X. Chen and K. Hu, *Eur. J. Med. Chem.*, 2012, **54**, 175–187.

26 P. V. M. D. Alan, *Cancer*, 2005, **103**, 2435–2446.

27 X. J. Zhu, Y. Shi, J. Peng, C. S. Guo, N. N. Shan, P. Qin, X. B. Ji and M. Hou, *Blood*, 2009, **114**, 5362–5367.

28 Y. G. Zheng, J. Su, C. Y. Gao, P. Jiang, L. An, Y. S. Xue, J. Gao and Y. Liu, *Eur. J. Med. Chem.*, 2017, **130**, 393–405.

29 H. Y. Lin, Z. K. Li, L. F. Bai, S. K. Baloch, F. Wang, H. Y. Qiu, X. Wang, J. L. Qi, R. W. Yang, X. M. Wang and Y. H. Yang, *Biochem. Pharmacol.*, 2015, **96**, 93–106.